Introductory lectures on QCD

B. Grinstein
University of California at San Diego, La Jolla, USA

Abstract
After describing the quark and parton models, we introduce QCD, explain factorization in perturbative QCD, and show how to derive evolution equations. We discuss violations of Bjorken scaling.

1 Introduction

Quantum chromodynamics (QCD) is firmly established as the theory of strong interactions. This formidable status was gained through a vast array of successes in explaining and predicting phenomena. It is a quantum field theory described by a deceptively simple Lagrangian. But despite this simplicity, QCD is a difficult theory to understand. Many techniques have been developed to analyze the predictions of the theory in a variety of contexts. Perturbative techniques are particularly suitable to study very high energy collisions [1]. Numerical simulation of QCD formulated on the lattice is particularly apt for computations of static or low energy quantities involving a few hadrons, like masses or near threshold form factors. Lattice QCD is also powerful in examining the thermal behaviour of QCD; this was the starting point of the lectures on quark–gluon plasma by U. Heinz in this school. Effective Lagrangians were developed [2, 3] to study the short distance modifications of the weak interactions that dictate the decays of light, charm and beauty hadrons. Other effective theories, like HQET [4, 5], NRQCD [6] and SCET [7], have been developed to study the effects of QCD and are currently the object of intense study.

These lectures are intended as an introductory presentation of the techniques of perturbative QCD. In the short time provided it is prudent to limit ourselves to this very practical topic, one that we feel is of most interest to the student of experimental particle physics. Hence, many other interesting subjects, including lattice QCD, chiral Lagrangians, instantons, anomalies, and the various recently developed effective theories are omitted. Even some more advanced subjects in perturbative QCD, like Sudakov re-summation and the BFKL equations, are left out. The intention is that a student who knows little or nothing about QCD will come out with a working understanding of how one performs computations of high energy cross-sections for production of, say, the top quark at the Tevatron or supersymmetric particles at the LHC.

Therefore, the reader should not look here for a comprehensive review of the current status of perturbative QCD, let alone the whole of QCD, in these lectures. Excellent reviews of the current status of QCD can be found in many lectures in recent CERN schools [8–12].

We will begin by reviewing the quark model and how colour was proposed as the solution of the Fermi–Dirac statistics problem. We will proceed then to a discussion of deep inelastic scattering (DIS) and introduce the parton model and Bjorken scaling. Only then will we present the QCD Lagrangian and discuss some of its properties, most saliently asymptotic freedom. Armed with this we will conclude by studying violations to Bjorken scaling. To this end we will give a simple presentation of factorization, and then of the evolution equations and their use in understanding the violations to Bjorken scaling. Along the way we will learn how to use the parton model to describe other processes, such as Drell–Yan and two-jet production in pp scattering.

2 The quark model

The quark model was introduced in 1963 by Gell-Mann and Zweig to explain the increasingly complex list of stable hadrons and hadronic resonances that had been discovered in the new particle accelerators of the 1950s and 1960s. It was known that isospin was a very good symmetry of the strong interactions

and that a $U(1)$ quantum number, a 'charge' called strangeness, was conserved by them. Moreover, these two symmetries had been combined into a larger, more predictive symmetry group, flavour-$SU(3)$, which was found to be conserved to a good approximation, but not exactly, by the strong interactions. The quark model was introduced to give a simple realization of this symmetry, and it is simplest to explain flavour-$SU(3)$, or $SU(3)_f$ for short, by introducing first the quark model itself.

The quark model describes mesons as bound states of a quark and an antiquark. Baryons, on the other hand, are composed of three quarks, and antibaryons of three antiquarks:

$$\begin{array}{ll} \text{mesons } (\pi\ K\ \rho\ \omega & \ ) = q\bar{q} \\ \text{baryons } (p\ n\ \Lambda\ \Xi & \ ) = qqq \end{array}$$

Since mesons have integer spin while baryons have half-integer spin, it was further posited that quarks have spin-1/2. One expects that the lowest mass mesons and baryons have vanishing spatial angular momentum.

- Mesons ($J^P = 0^-\ 1^-$):
  - spin-singlet ($\frac{1}{\sqrt{2}}(\uparrow\downarrow - \downarrow\uparrow)$) with $L = 0$,
  - spin-triplet ($\uparrow\uparrow$, $\frac{1}{\sqrt{2}}(\uparrow\downarrow + \downarrow\uparrow)$, $\downarrow\downarrow$) with $L = 0$.

For the baryons we could in principle have all combinations of three spin-1/2 quarks:

$$1\ \ 2 \times 1\ \ 2 \times 1\ \ 2 = 1\ \ 2 \times (0 + 1) = 1\ \ 2 + 1\ \ 2 + 3\ \ 2 \tag{1}$$

To get the right spectrum of baryons we further assume that their wave-function is totally symmetric in quark spin. This eliminates one spin-1/2 term in the decomposition above and we have the following:

- Baryons ($J^P = 1\ \ 2^+\ \ 3\ \ 2^+$):
  - spin-1 $\ 2$ with $L = 0$,
  - spin-3 $\ 2$ with $L = 0$.

Three types, or *flavours,* of quarks (up, down, and strange, or u, d, and s) were necessary to explain the spectrum of hadrons then known. Today we know there are a further three quarks, the charm, bottom, and top (c, b, and t). These 'heavy' quarks could not be produced in the accelerators existing in the 1960s and their behaviour in QCD is significantly different because their mass is significantly larger than 300 MeV, the scale characterizing the strong interactions. In these lectures we will be mainly concerned with the light quarks.

In terms of the three light quarks, the quark content of the proton is uud and of the neutron is udd. In order to explain the charge of these baryons, the u and d quarks are assigned charges $2\ \ 3$ and $-1\ \ 3$, respectively. The light pseudo-scalar mesons π^+ and π^- have quark content $u\bar{d}$ and $d\bar{u}$. The neutral partner of these, the π^0, is a linear combination of $u\bar{u}$ and $d\bar{d}$. We will present the specific linear combination when we introduce isospin and require that the three mesons form an isospin triplet. Pseudo-scalar mesons with strangeness must include the strange quark or its antiquark. Thus, the quark assignment of the K^+ and K^0 is $u\bar{s}$ and $d\bar{s}$, so s must have charge $-1\ \ 3$.

The $SU(3)_f$ symmetry can now be easily described. Arrange the three quarks into a column vector and define it to transform as a triplet, **3**, that is, as the fundamental representation of $SU(3)$,

$$\begin{pmatrix} u \\ d \\ s \end{pmatrix} \to U \begin{pmatrix} u \\ d \\ s \end{pmatrix} \qquad U \in SU(3) \tag{2}$$

The group of $N \times N$ matrices U that are unitary ($U^\dagger U = 1$) is called $U(N)$. It follows from $U^\dagger U = 1$ that $|\det U|^2 = 1$, that is, $\det U = e^{i\phi}$, a pure phase. If we restrict the matrices further by the condition $\det U = 1$ we have the group $SU(N)$. It follows that $U(N)$ is the product of the groups $SU(N)$ and $U(1)$, the group of pure phases. The case of interest for us here is $SU(3)$. $N = 3$ because we have three light quarks, and $SU(3)$ rather than $U(3)$ because the additional $U(1)$ factor is an exact symmetry of QCD, namely baryon number.

Isotopic spin, or *isospin* symmetry, and strangeness are embedded in $SU(3)_f$ in a simple way. Isospin is the symmetry

$$\begin{pmatrix} u \\ d \end{pmatrix} \to U \begin{pmatrix} u \\ d \end{pmatrix} \qquad U \in SU(2) \tag{3}$$

while strangeness is a $U(1)$ symmetry

$$s \to Us \qquad U \in U(1) \tag{4}$$

We can now understand how elementary particles fall into representations of $SU(3)_f$. Consider the case of mesons, containing a quark, a member of the **3** representation, and an antiquark, a $\bar{\mathbf{3}}$. The product of these decomposes as

$$\mathbf{3} \times \bar{\mathbf{3}} = \mathbf{8} + \mathbf{1} \tag{5}$$

This accounts for the two meson octets,

- $J^P = 0^-$: $(\pi^\pm \ \pi^0 \ K^\pm \ K^0 \ \bar{K}^0 \ \eta)$
- $J^P = 1^-$: $(\rho^\pm \ \rho^0 \ K^{*\pm} \ K^{*0} \ \bar{K}^{*0} \ \omega)$,

and two meson singlets, the η' and ω', with $J^P = 0^-$ and $J^P = 1^-$, respectively. It is easy to work out the quark content of each meson. The three states π^+, K^+ and K^0 have content $u\bar{d}$, $u\bar{s}$ and $d\bar{s}$, and their three antiparticles have the corresponding anti-content. The only subtlety is with the neutral states $\pi^0 = (u\bar{u} - d\bar{d})\ \sqrt{2}$ and $\eta = (u\bar{u} + d\bar{d} - 2s\bar{s})\ \sqrt{6}$, which are chosen this way to make the π^0 a member of an isospin triplet with the $\pi^p m$ and the η an isospin singlet. The η' has content $(u\bar{u} + d\bar{d} + s\bar{s})\ \sqrt{3}$, a singlet under $SU(3)_f$. Because the symmetry is not exact, the physical π^0, η and η' are small admixtures of the three quark decompositions given here.

For the baryons we have the decomposition

$$\mathbf{3} \times \mathbf{3} \times \mathbf{3} = \mathbf{10} + \mathbf{8} + \mathbf{8} + \mathbf{1} \tag{6}$$

but have the additional rule, encountered when considering spin, that the wave-function is totally symmetric. So the states that remain are as follows.

- Baryon octet, $J^P = 1\ 2^+$: $(p \ n \ \Sigma^\pm \ \Sigma^0 \ \Xi^- \ \Xi^0 \ \Lambda)$.
- Baryon decouplet, $J^P = 3\ 2^+$: $(\Delta^{++} \ \Delta^+ \ \Delta^0 \ \Delta^- \ \Sigma^\pm \ \Sigma^0 \ \Xi^- \ \Xi^0 \ \Omega^-)$.

The reader can easily work out the quark content given the charges and strangeness of each particle.

The quark model successfully accommodates all these particles and resonances. A remarkable success of the $SU(3)_f$ was the prediction, including the mass, of the $\Omega^- = sss$ baryon. But the model has its problems. The first, most obvious problem is that no matter how hard physicists have tried, a free quark has never been observed. Is the quark a real particle or simply a mathematical construct that allows us to keep track of $SU(3)_f$ in an efficient manner? A second problem is the absence of antisymmetric combinations of spin and of flavour representations in the baryon sector. This is not unrelated to a third problem, that of Fermi–Dirac statistics. Baryons, having an odd number of spin-1/2 components, should have totally antisymmetric wave-functions. Since they have $L = 0$, their spatial wave-functions are symmetric, and we have imposed that their spin and flavour wave-function factors be symmetric too.

Therefore, the wave-functions are totally symmetric. This is most easily seen in the Δ^{++}, which is a $J^P = 3\ \ 2^+$ baryon with content $u^\uparrow u^\uparrow u^\uparrow$ that is explicitly totally symmetric.

To solve the Fermi–Dirac statistics problem, Han and Nambu, Greenberg and Gell-Mann, independently proposed adding an additional quantum number to the quarks. The Fermi–Dirac problem is solved if we assume that baryon wave-functions are antisymmetric under this new quantum number, named *colour*. Since the wave-functions are symmetric under space, spin and flavour, antisymmetry in colour gives totally antisymmetric wave-functions. For this to work we need three different colour labels for the quarks. So instead of having a u quark, there are three u quarks, labelled u_i with $i = 1\ \ 2\ \ 3$, and similarly for d and s. There is therefore a new internal symmetry that rotates the colour degrees of freedom among themselves, and since there are three colours, the symmetry group is $SU(3)$. To distinguish this from flavour we will denote it $SU(3)_c$.

To summarize, there are two different sets of transformations:

- $SU(3)_f$ transforms $u_i \leftrightarrow d_i \leftrightarrow s_i$,
- $SU(3)_c$ transforms $u_1 \leftrightarrow u_2 \leftrightarrow u_3$.

In fact *the* quark q carries both quantum numbers: q_{ai} with $a = u\ \ d\ \ s$ and $i = 1\ \ 2\ \ 3$. It transforms as a $(3\ \ 3)$ under $SU(3)_f \times SU(3)_c$, which act as follows.

- $SU(3)_f$: $q_{ai} \to U^b_a q_{bi}, U \in SU(3)_f$.
- $SU(3)_c$: $q_{ai} \to U^j_i q_{aj}, U \in SU(3)_c$.

The Fermi–Dirac statistics problem has then an elegant solution. We postulate that hadrons are invariant under $SU(3)_c$. To see how this works we first show that the antisymmetric combination of colours is invariant. To this end consider the totally antisymmetric three-index symbol, ϵ_{ijk} with the convention $\epsilon_{123} = 1$. Note that

$$U^l_i U^m_j U^n_k \varepsilon_{lmn} = \varepsilon_{ijk} \det U = \varepsilon_{ijk} \tag{7}$$

which is equivalent to the statement that it is invariant:

$$\varepsilon_{ijk} \to U^l_i U^m_j U^n_k \varepsilon_{lmn} = \varepsilon_{ijk} \tag{8}$$

It is now straightforward to construct invariant wave-functions:

$\bar{q}^{ai} q_{bi}$	$\varepsilon^{ijk} q_{ai} q_{bj} q_{ck}$	$\varepsilon_{ijk} \bar{q}^{ai} \bar{q}^{bj} \bar{q}^{ck}$
(mesons)	(baryons)	(anti-baryons)

While this is an elegant solution to the statistics problem, it introduces new problems and leaves us with some of the old ones.

- Why $SU(3)_c$? Is this an accidental symmetry. Introducing this seems artificial.
- The statement that 'hadrons are invariant under $SU(3)_c$' has replaced the *ad hoc* recipe that baryon wave-functions must be symmetric under spin and flavour, as well as spatially symmetric. But this new recipe is seemingly as *ad hoc* as the old one it replaces.
- We have still not resolved the free quark issue. However, since we are excluding particles that are not invariant under colour from the spectrum, the issue for free quarks would be solved if the *ad hoc* assumption of the previous item could be justified.
- We have no theory of strong interactions.

All of these problems are solved at once if we promote the global $SU(3)_c$ symmetry to a local symmetry. A theory with local $SU(3)$ symmetry requires a new vector boson with dynamics described by the Yang–Mills Lagrangian. This vector boson mediates forces and is therefore a candidate for a theory of strong interactions. Moreover, the theory is now known to exhibit the property of confinement, that is, that free quarks cannot exist, and only colour invariants are to be found in the spectrum. Finally, $SU(3)_c$ is no longer accidental, rather it gives rise to the dynamics of the strong interactions. As we will see, there is an added dividend: a theory of strong interactions based on $SU(3)$ Yang–Mills exhibits the property of asymptotic freedom which, as we will see, is necessary to understand the results of deep inelastic experiments that were underway at the time the quark theory was being developed.

3 The parton model

When protons collide with protons at the moderate energies that were available in the particle accelerators of the 1960s, the particles that emerge from the collision, mostly pions, are largely collinear with the original protons. This is suggestive of a picture of hadrons as complex systems of softly bound particles like pions.

However, when energetic electrons collide with protons a different picture emerges. In the SLAC–MIT deep inelastic scattering (DIS) experiment of the 1960s it was seen that there is a significant rate for e^- scattering at large angles as if protons were elementary. This is reminiscent of Rutherford's experiment in which the atomic nucleus was discovered. However, rarely was there a single proton in the final state. It was in an effort to reconcile the soft behaviour of pp scattering with the hard behaviour in DIS that Feynman, and Bjorken and Paschos independently proposed the parton model [18, 19].

3.1 DIS kinematics

In DIS we are interested in the distribution of outgoing electrons in the process $e^- + H \to e^- + X$ where H is a hadron, typically a proton, neutron or deuteron, and the X in the final state indicates that we do not keep track of the hadronic final state. Figure 1 represents the process and indicates the kinematic variables. In all our diagrams time runs from left to right. As the figure indicates, the interaction consists of a photon exchange between the electron and a target constituent, or *parton*. The incoming and outgoing electrons have energy E and E', respectively. The four momentum is chosen so that the incoming electron is moving in the z direction, $k = E(1\ 0\ 0\ 1)$, while the outgoing electron has arbitrary direction, $k' = E'(1\ \sin\theta\cos\phi\ \sin\theta\sin\phi\ \cos\theta)$ (we can choose the xy axes so that $\phi = 0$ if we wish). In the rest-frame of the hadron $P = M(1\ 0\ 0\ 0)$. The photon carries momentum $q = k - k'$. Two convenient dimensionless variables are

$$x \equiv -\frac{q^2}{2P\cdot q} \qquad\qquad y \equiv \frac{2P\cdot q}{2P\cdot k} \tag{9}$$

Computing

$$q\cdot P = M(E'-E) \qquad q^2 = -2k\cdot k' = -2EE'(1-\cos\theta) \tag{10}$$

we see that y measures the energy of the photon, while x is a measure of the 'off-shellness' of the photon (relative to energy).

It will be useful to express cross-sections in terms of Mandelstam variables. For any process of the type $1 + 2 \to 1' + 2'$, see Fig. 2, we define Mandelstam variables as the three Lorentz invariants

$$s = (p_1 + p_2)^2 \tag{11}$$
$$t = (k_1 - p_1)^2 \tag{12}$$
$$u = (k_2 - p_1)^2 \tag{13}$$

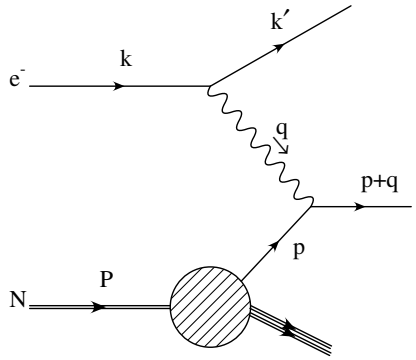

Fig. 1: Diagram showing the kinematic variables for deep inelastic eN scattering. The electron of initial momentum k scatters into momentum k' off a parton with momentum p, a fraction of the nucleon's momentum P.

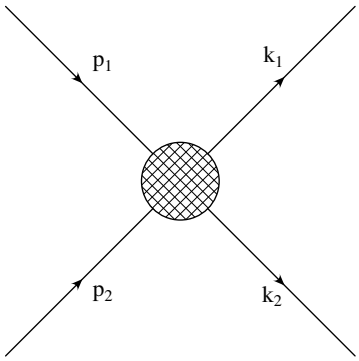

Fig. 2: Mandelstam variables are defined for any process of the type $1 + 2 \to 1' + 2'$

The three variables are not independent. If the masses of the particles are m_i, $i = 1 \quad 4$, then $s + t + u = m_1^2 + m_2^2 + m_3^2 + m_4^2$. In the case that all masses are negligible, $s + t + u = 0$.

In DIS we will be concerned only with measuring the outgoing electron, ignoring the details of the hadronic final state. Therefore, experimentally we measure the final momentum k' or, equivalently, q. Below we will relate the cross-section for the underlying electron–parton scattering to the cross-section for $e^- H \to e^- X$. So let us consider the relation between the kinematic variables for this to the one for the underlying parton collision. It is customary to introduce a positive variable $Q^2 \equiv -q^2 > 0$. It is easy to see that q^2 is negative:

$$q^2 = -2k \cdot k' = -2EE'(1 - \cos\theta) < 0 \tag{14}$$

The t variable for the parton collision is

$$\hat{t} = -Q^2 \tag{15}$$

As is customary, we will differentiate the partonic variables by placing a hat over them. We see that the parton variable $\hat{t}$ is simply the corresponding variable $t = -Q^2$ of the $e^- H$ scattering process.

Computing $\hat{s}$ is less straightforward. When the energy of the collision is large the target mass can be neglected. One can consider the collision in, for example, the centre of mass frame. When the energy is large the target momentum approximates that of a massless particle. The partons are also to good approximation massless. This provides a nice picture: since all partons are massless they can travel together, at the speed of light, even though they carry different energies. Moreover, the direction of travel is that of the parent hadron, so their four momentum is just proportional to the momentum of the parent hadron. In Fig. 1 the momentum of the parton participating in the collision is p. Since this is collinear

with the proton momentum, P, we write

$$p = \xi P \tag{16}$$

where ξ, $0 \leq \xi \leq 1$, is the collinear momentum fraction of that parton. Now,

$$\hat{s} = (p+k)^2 = 2p \cdot k = 2\xi P \cdot k = \xi s \tag{17}$$

that is,

$$\hat{s} = \xi s \tag{18}$$

There is one more interesting relation. Because the outgoing parton carries negligible mass its momentum must be light-like, $(p+k)^2 = 0$. It follows that

$$2p \cdot q + q^2 = 2\xi P \cdot q - Q^2 = 0 \tag{19}$$

Therefore we have the remarkable relation between the momentum fraction of the struck parton, ξ, and the kinematic variable x for the $e^- H$ collision introduced earlier:

$$\xi = \frac{Q^2}{2P \cdot q} = x \tag{20}$$

3.2 Parton densities and Bjorken scaling

To compute the DIS cross-section we introduce parton densities, defined so that $f_i^H(\xi)d\xi$ gives the probability to find parton i in the hadron *H* with momentum fraction within $d\xi$ of ξ. The probability of scattering off the hadron is the sum over probabilities of scattering off the parton components:

$$\frac{d\sigma}{d\hat{t}}(e(k)H(P) \to e(k')X) = \sum_i \int d\xi \, f_i(\xi) \frac{d\hat{\sigma}}{d\hat{t}}(e(k)q_i(p) \to e(k')q_i) \tag{21}$$

The cross-section $d\hat{\sigma}$ for parton–e^- scattering is just like for $\mu^- e^-$ scattering, except that the charge of the *i*th parton is not unity. If e_i denotes this charge, and using $\xi = x$, we then have

$$\frac{d\sigma}{dQ^2 dx} = \sum_i f_i(x) e_i^2 \frac{2\pi\alpha^2}{Q^4} \left[1 + \left(1 - \frac{Q^2}{xs} \right)^2 \right] \tag{22}$$

We notice immediately that up to the explicit factor of $[1 + (1 - Q^2 \ xs)^2] \ Q^4$ the cross-section is independent of Q^2, a phenomenon known as Bjorken scaling. The x-dependence is through the combination $\sum_i e_i^2 f_i(x)$ which depends on the target structure and is difficult to compute since it involves non-perturbative dynamics. Figure 3 shows the DIS cross-section for a proton target divided by $[1 + (1 - Q^2 \ xs)^2] \ Q^4$ as a function of x. Data are shown for different Q ranging from 7.0 GeV to 19.5 GeV. That all these fall on the same line is striking confirmation of Bjorken scaling. As we will see in a later chapter, the contemporary emphasis is on *violations* of scaling, so the modern counterparts of the graph in Fig. 3 display separately data for different values of Q. The reader can easily produce a graph similar to that in Fig. 3 by starting from the data in, for example, Fig. 18.

The success of the parton model hinges on the separation of time scales for the parton collision process and the parton mutual interactions in the target, say, a proton. The electron can interact with partons only while it traverses the proton. The size of the proton is about a fermi, or roughly m_p^{-1}. But the fast off-shell photon sees a Lorentz-contracted proton in the direction it is travelling. The relativistic dilation factor for a massive particle is $\gamma = E \ m$; Q plays the role of the mass for the off-shell photon of energy q^0. Thus the time available for the interaction is $T_{\gamma q} \sim m_p^{-1}(Q \ q^0) = Q \ P \cdot q = 2x \ Q \sim 1 \ Q$. The typical time for parton–parton interaction in the proton is given by the time it takes for a parton to traverse the proton, $T_{qq} \sim m_p^{-1}$. The DIS condition $Q \gg m_p$ gives $T_{qq} \gg T_{\gamma q}$. The correct theory

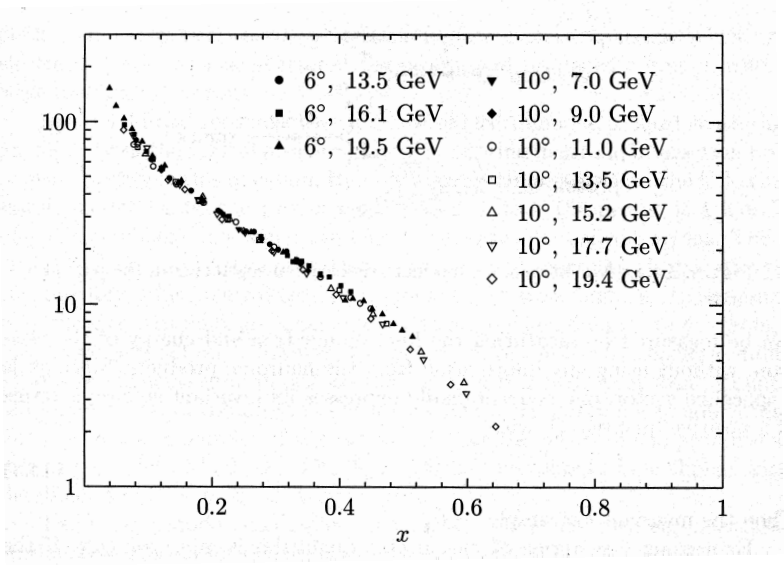

Fig. 3: Test of Bjorken scaling: inclusive cross-section for ep scattering, divided by the Q^2-dependent factor in Eq. (22), as a function of the dimensionless variable $x \equiv Q^2/2P \cdot q$, for a variety of electron scattering angles and values of Q. The figure is taken from the textbook by Peskin and Schroeder [15].

of strong interactions must be such that it exhibits strong binding forces over time or distance scales of the order of a fermi, but is weak, as if the partons were free, over time or distance scales much shorter. Happily, this necessary property of the interactions is exhibited by QCD, which is 'asymptotically free': the force it mediates grows weaker with shorter interaction times.

Electron scattering probes the combination $\sum_i e_i^2 f_i^H(x)$, but how can one obtain information on the individual parton densities $f_i(x)$? There are general constraints that follow from flavour conservation of the strong interactions. Since the proton contains two up quarks, one down quark and no strange quarks, it follows that

$$\int_0^1 d\xi[u(\xi) - \bar{u}(\xi)] = 2 \qquad \int_0^1 d\xi[d(\xi) - \bar{d}(\xi)] = 1 \qquad \int_0^1 d\xi[s(\xi) - \bar{s}(\xi)] = 0 \tag{23}$$

We use $f_i^p(x) = f_i(x)$ and make the superscript explicit only for other targets. Furthermore, we will often use the simpler notation $f_u(x) = u(x)$, etc. Since the longitudinal momentum of the partons must add up to the longitudinal momentum of the proton we have a momentum sum rule

$$\int_0^1 d\xi\, \xi[u(\xi) + d(\xi) + s(\xi) + \bar{u}(\xi) + \bar{d}(\xi) + \bar{s}(\xi) + g(\xi)] = 1 \tag{24}$$

Here we have anticipated a gluon component of the proton, $f_g(x) = g(x)$, and above we had already introduced an antiquark component.

Since the neutron is related to the proton by isospin, we replace $u \leftrightarrow d$ in going from f^p to f^n:

$$f_u^n(\xi) = f_d(\xi) \qquad f_d^n(\xi) = f_u(\xi) \qquad f_{\bar{u}}^n(\xi) = f_{\bar{d}}(\xi) \qquad f_{\bar{d}}^n(\xi) = f_{\bar{u}}(\xi) \qquad f_s^n(\xi) = f_s(\xi) \tag{25}$$

There are similar relations for the antiproton parton densities, $f_{\bar{u}}^{\bar{p}} = f_u$, $f_u^{\bar{p}} = f_{\bar{u}}$, etc.

What should we expect for these densities? A naïve guess is that each of the three so called *valence* quarks of the proton (uud) carries a third of the momentum, so $d(\xi) = u(\xi)\ 2 = \delta(\xi - 1\ 3)$. However

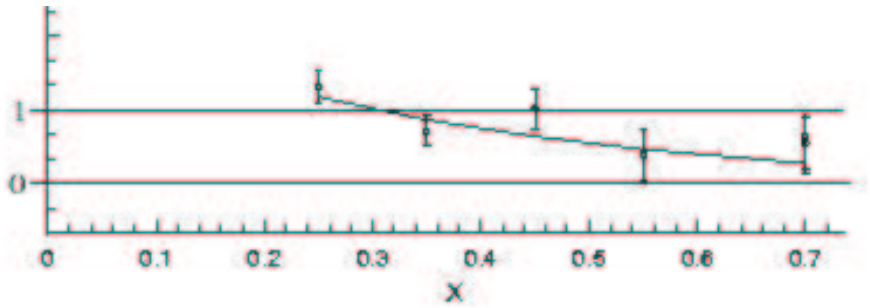

Fig. 4: Ratio of neutron to proton cross-sections at $Q = 10$ GeV in muon DIS from the NMC experiment. The curve is the prediction of CTEQ3M parton densities [20].

interactions between them should smear out the delta function. Moreover, since valence quarks can radiate quark-antiquark pairs we should expect some small component of these *sea* quarks, which should be approximately flavour independent. Also, their density should be concentrated at small values of ξ since they are produced from radiation from a valence quark which had only a fraction of longitudinal momentum to begin with and is shared between the resulting pair and the valence quark. Similarly, we expect the glue component to be concentrated at small ξ.

We can begin to verify these expectations by comparing the neutron and proton DIS cross-sections. Consider their ratio:

$$\frac{\frac{d^2\sigma}{dxdy}(en \to eX)}{\frac{d^2\sigma}{dxdy}(ep \to eX)} = \frac{\left(\frac{2}{3}\right)^2[d+\bar{d}] + \left(\frac{1}{3}\right)^2[u+\bar{u}] + \left(\frac{1}{3}\right)^2[s+\bar{s}]}{\left(\frac{2}{3}\right)^2[u+\bar{u}] + \left(\frac{1}{3}\right)^2[d+\bar{d}] + \left(\frac{1}{3}\right)^2[s+\bar{s}]} \tag{26}$$

This satisfies a strict bound,

$$\frac{1}{4} \leq \frac{\frac{d^2\sigma}{dxdy}(en \to eX)}{\frac{d^2\sigma}{dxdy}(ep \to eX)} \leq 4 \tag{27}$$

where the upper and lower bounds correspond to d and u dominance, respectively. Moreover, if the sea quarks are dominant, all densities should be similar and the ratio should approach unity. Figure 4 shows the experimental ratio. It is seen that at large $x = \xi$ the ratio approaches the lower bound, where the u quark dominates, while at small x we see the ratio close to one, which corresponds to sea dominance.

From the difference of these cross-sections

$$\frac{d^2\sigma}{dxdQ^2}(ep \to eX) - \frac{d^2\sigma}{dxdQ^2}(en \to eX) = \frac{2\pi\alpha^2}{Q^4}\left[1 + \left(1 - \frac{Q^2}{xs}\right)^2\right]\frac{1}{3}[u(x) - d(x)] \tag{28}$$

we can infer the difference between up and down densities. Since we expect $u(x) \approx 2d(x)$ this directly measures the valence contributions. Notice that the quark sea contribution cancels in the difference. The plot in Fig. 5 shows the difference in cross-sections divided by $2\pi\alpha^2\ xQ^4[1 + (1 - Q^2\ xs)^2]$, which equals $1\ 3[xu(x) - xd(x)] \approx 1\ 3\, xd(x)$ in the parton model. We therefore expect it to peak around $x = 1\ 3$ and have height of about $1\ 3x \approx (1\ 3)(1\ 3) = 1\ 9$.

Additional information on parton densities can be inferred from other processes in which the cross section is given in terms of a different combination of densities. Consider, for example, neutrino DIS experiments:

$$\frac{d^2\sigma}{dxdy}(\nu p \to \mu^- X) = \frac{G_F^2}{\pi}\, s\, [xd(x) + x\bar{u}(x)(1-y)^2] \tag{29}$$

Since this proceeds through W^+ exchange, the struck parton must produce a parton with one more unit of electric charge. This can happen for the d quark, $(d + W^+ \to u)$, or for $\bar{u}$, $(\bar{u} + W^+ \to \bar{d})$, but not

for u or $\bar{d}$. The additional factor of $(1-y)^2$ arises from the fact that the $\nu \to \mu^-$ and $d \to u$ vertices involve left-handed particles, while the antiquark vertex involves right-handed ones. Similarly,

$$\frac{d^2\sigma}{dxdy}(\bar{\nu}p \to \mu^+ X) = \frac{G_F^2}{\pi}\, s\, [xu(x)\,(1-y)^2 + x\bar{d}(x)] \tag{30}$$

These expressions should be modified to account for Cabibbo mixing. This is easily accomplished by replacing $d \to \cos^2\theta_C d + \sin^2\theta_C s$.

A set of parton densities obtained by a global fit to experiments by the CTEQ collaboration is shown in Fig. 6. We see valence quark densities peaking at $x \approx 1\ 3$ and sea and gluon densities becoming important at small x.

4 QCD

When combining the successes of the quark and parton model we are driven to adopt a Yang–Mills theory in which the global colour symmetry is elevated to a local symmetry. The symmetry group is $SU(3)_c$. Fermion fields that carry colour quantum numbers, a.k.a. quarks,

$$\psi(x) = \begin{pmatrix} \psi_1(x) \\ \psi_2(x) \\ \psi_3(x) \end{pmatrix}$$

transform as $\psi(x) \to U(x)\psi(x)$ where $U(x) = e^{i\omega^a(x)T^a}$. The 'generators' T^a are 3×3 hermitian matrices. Hermiticity follows by insisting that the group matrices U be unitary, $U^\dagger U = 1$, while keeping the parameters of the local transformation, $\omega^a(x)$, real. The generators of $SU(3)$ are traceless; a trace would generate the $U(1)$ subgroup of $U(3)$ that is absent in $SU(3)$. Hence the label a runs over eight values, $a = 1 \qquad 3^2 - 1 = 8$.

The Lie algebra is defined by the commutation relations

$$[T^a\ T^b] = if^{abc}T^c \tag{31}$$

in which the structure constants f^{abc} are real and antisymmetric in the indices a, b and c. The normalization of the structure constants fixes the trace and Casimir invariants for any representation R:

$$\mathrm{Tr}(T^aT^b) = C(R)\delta^{ab} \qquad\qquad \sum T^aT^a = C_2(R)\cdot\mathbf{1} \tag{32}$$

For the 'defining' or 'fundamental' representation of the quarks, $C(\text{fund}) = 1\ 2$ and $C_2(\text{fund}) = 4\ 3$, while for the adjoint representation, to which gluons belong, $C(\text{Adj}) = C_2(\text{Adj}) = 3$. A very useful identity to which we will refer as 'a very useful identity' is $\sum_a (T^a)_{ij}(T^a)_{kl} = 1\ 2\delta_{il}\delta_{kj} - 1\ 6\delta_{ij}\delta_{kl}$.

The covariant derivative

$$D_\mu\psi(x) = (\partial_\mu - igT^aA_\mu^a)\psi(x) \tag{33}$$

is defined so that $D_\mu\psi(x)$ transforms homogeneously, $D_\mu\psi(x) \to U(x)D_\mu\psi(x)$, just like the field ψ, $\psi(x) \to U(x)\psi(x)$. To accomplish this we must take care to choose appropriate transformation rules for the gauge field A_μ^a. These are most succinctly expressed in terms of the matrix of gauge fields $A_\mu \equiv A^a(x)T^a$:

$$A_\mu \to U(x)(A_\mu - \frac{i}{g}\partial_\mu)U^\dagger(x) \tag{34}$$

The gauge-field kinetic energy is most readily expressed in terms of the gauge-field strength $F_{\mu\nu}^a$. In matrix notation, $F_{\mu\nu} = 1\ - ig[D_\mu\ D_\nu] = \partial_\mu A_\nu - \partial_\nu A_\mu - ig[A_\mu\ A_\nu]$ and explicitly

$$F_{\mu\nu}^a = \partial_\mu A_\nu^a - \partial_\nu A_\mu^a + gf^{abc}A_\mu^b A_\nu^c \tag{35}$$

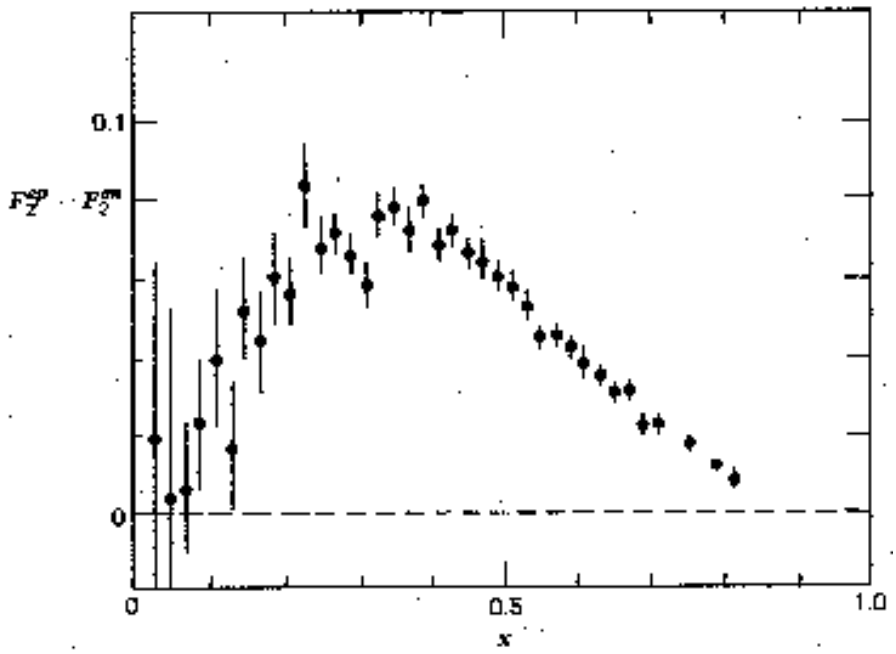

Fig. 5: Difference of neutron and proton deep inelastic scattering cross-sections. The Q^2-dependent factor in Eq. (28) has been divided out to give simply $\frac{1}{3}(xu(x) - xd(x)) \approx \frac{1}{3}\,xd(x)$. The graph was taken from the text by Halzen and Martin [16].

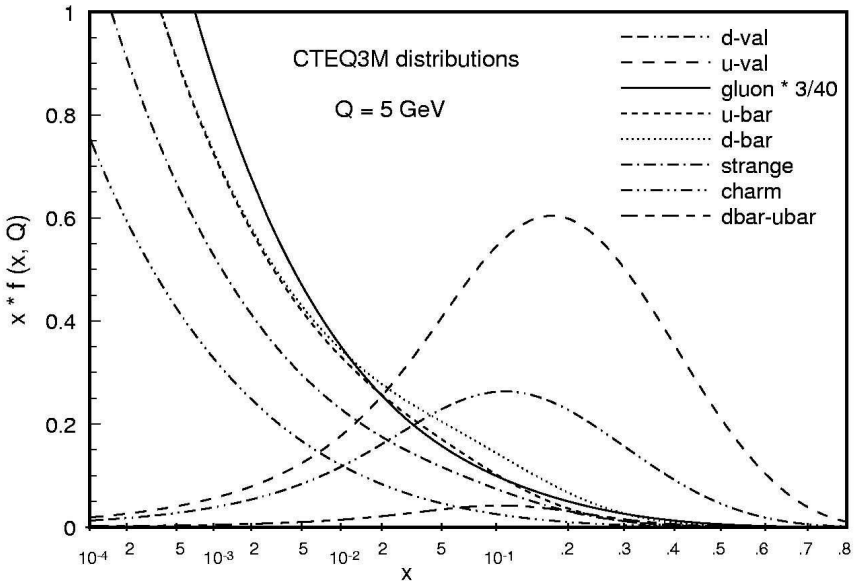

Fig. 6: CTEQ3M parton densities obtained through a global fit by the CTEQ Collaboration [20].

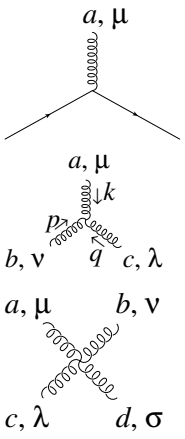

$$= \quad ig\gamma^\mu T^a$$

$$= \quad gf^{abc}[g^{\mu\nu}(k-p)^\lambda + g^{\nu\lambda}(p-q)^\mu + g^{\lambda\mu}(q-k)^\nu]$$

$$= \quad \begin{aligned} -ig^2[&f^{abe}f^{cde}(g^{\mu\lambda}g^{\nu\sigma} - g^{\mu\sigma}g^{\nu\lambda}) + \\ &f^{ace}f^{bde}(g^{\mu\nu}g^{\lambda\sigma} - g^{\mu\sigma}g^{\nu\lambda}) + \\ &f^{ade}f^{bce}(g^{\mu\nu}g^{\lambda\sigma} - g^{\mu\lambda}g^{\sigma\nu})] \end{aligned}$$

Fig. 7: Feynman rules for QCD

The QCD Lagrangian (including only one quark of mass m, for simplicity) is

$$\mathcal{L} = -\frac{1}{4}F^a_{\mu\nu}F^{a\mu\nu} + \overline{\psi}^j(i\not{D}^k_j - m\delta^k_j)\psi_k = -\frac{1}{2}\mathrm{Tr}F^2 + \overline{\psi}(i\not{D} - m)\psi \tag{36}$$

We have written colour indices explicitly first, and then implicitly. The latter notation is common and efficient, but less transparent. The interaction terms follow by expanding all terms:

$$\mathcal{L} = \mathcal{L}_0 + gA^a_\mu\bar{\psi}\gamma^\mu T^a\psi - gf^{abc}(\partial_\mu A^a_\nu)A^{b\mu}A^{c\nu} - g^2 f^{eab}f^{ecd}A^a_\mu A^b_\nu A^{c\mu}A^{d\nu} \tag{37}$$

Here $\mathcal{L}_0$ is quadratic in the fields (includes kinetic energy and mass terms) and the next three terms give a fermion–fermion–gluon vertex, and triple and quadruple gluon vertices. The corresponding Feynman rules follow immediately and are listed in Fig. 7. We have omitted a discussion of ghost fields, which are necessary when computing loop graphs in QCD in order to maintain unitarity. We will not have occasion to compute loop graphs in these lectures. For more on this see, for example, Refs. [15,17].

When we assume that N_f massless quarks are included, the Lagrangian exhibits a large global symmetry, $U(N_f)_V \times U(N_f)_A$, where the first factor consists of 'vector' transformations (that is, they rotate left- and right-handed fermions the same), $\psi_f \to (e^{i\epsilon^a t^a})^{f'}_f \psi_{f'}$, and the second factor has axial transformations (counter-rotating left and right), $\psi_f \to (e^{i\epsilon^a t^a\gamma_5})^{f'}_f \psi_{f'}$. An overall phase rotation that corresponds to the $U(1)$ subgroup of $U(N_f)$ is simply baryon number, and the overall axial phase is the famous $U(1)_A$: it is a symmetry of the classical theory but not of the quantum theory. In nature, only three quarks are light enough for this approximate massless limit to be useful. The strong interaction dynamics spontaneously break the $SU(3)_V \times SU(3)_A$ flavour symmetry group to the $SU(3)_V$ subgroup, the flavour group of Gell-Mann and Ne'eman. The eight goldstone bosons of the spontaneously broken $SU(3)_A$ are identified with the octet of pseudoscalar mesons. This story is continued in Prof. Gavela's lectures in this school, but we now turn our attention to the perturbative dynamics of QCD.

A number of simple calculations allow us to verify that indeed there are only three colours in QCD. Consider the decay of a charged electroweak vector boson. It can decay to a lepton–neutrino pair, or N_c copies, one for each colour, of an up–down quark pair or of a strange–charm quark pair. Since the mass of all these objects is small compared to the mass of the W^- boson, differences in phase space are negligible. So we obtain $\mathrm{Br}(W \to e\nu) = 1\ (3 + 2N_c) = 11\%$, where the numerical value corresponds to $N_c = 3$ and is in excellent agreement with experiment. Similarly one obtains $\mathrm{Br}(\tau \to e\bar{\nu}_e\nu_\tau) = 1\ (2 + N_c) = 20\%$, which is in fairly good agreement with experiment, and the agreement improves when the effects of limited phase space are included. The ratio of cross-

sections $R = \sigma(e^+e^- \to \text{hads})\ \ \sigma(e^+e^- \to \mu^+\mu^-) = N_c \sum_i q_i^2$ is computed similarly. For centre-of-mass energies above charm–anticharm pair production threshold but below bottom–antibottom, we have $R = N_c\,(2\,1\ \ 9 + 2\,4\ \ 9)$, while above bottom $R = N_c\,(3\,1\ \ 9 + 2\,4\ \ 9)$. The cross-section does jump from $R \approx 2$ to $R \approx 7\ \ 3$ as the centre-of-mass energy increases from below to above the bottom pair production threshold.

These 'counting' calculations do not include the effects of QCD interactions, and one is led to ask how then are the results modified. Let us consider, for example, the ratio of hadronic to muonic cross-sections R. This is an example of an 'infrared safe' quantity, which means, roughly speaking, that when the external kinematic variables (here the centre of mass energy) are kept large and fixed as the quark masses are set to vanish no divergences are encountered. It is always the case that infrared safe quantities are 'inclusive' (in our case we add over all possible hadronic final states), although not every inclusive quantity is necessarily infrared safe. Infrared safe quantities have a perturbative expansion unencumbered by large, diverging logarithms of small masses (which of course render perturbation theory for non-safe quantities useless). We can safely set to zero the quark masses in any expression for an infrared safe quantity, the corrections being a small effect. So infrared safe quantities F are functions of the large external kinematic variables, which I collectively denote by E, the coupling constant $\alpha_s = g_s^2\ \ 4\pi$ and, since QCD is a renormalizable field theory, the renormalization scale μ: $F = F(E\ \ \mu\ \ \alpha_s)$.

Physical quantities are independent of the arbitrary choice of μ. If the infrared safe quantity F is a physical observable, then we must have $\mu dF\ \ d\mu = 0$. This does not mean that F does not have explicit μ dependence, but rather it is cancelled by the implicit dependence (through the definition of the coupling constant, g_s). Hence we have the renormalization group equation (RGE):

$$\mu \frac{d}{d\mu} F = \left(\mu \frac{\partial}{\partial \mu} + \beta(g_s) \frac{\partial}{\partial g_s} \right) F(E\ \ \mu\ \ g_s) = 0 \tag{38}$$

Here $\beta(g_s)$ is the beta function of QCD and describes the implicit μ dependence in g_s. It can be computed in perturbation theory, and to leading order $\beta(g_s) = -(b_0\ \ 16\pi^2) g_s^3 + \mathcal{O}(g_s^5)$, with $b_0 = 11 - 2\ \ 3n_f$ where n_f is the number of active flavours. To solve the RGE it will be useful to introduce the running coupling $\bar{g}_s(t)$ as a solution to the equation

$$\frac{d\bar{g}_s}{dt} = \beta(\bar{g}_s(t)) \tag{39}$$

with boundary condition $\bar{g}_s(0) = g_s$. For example, keeping only the leading term in β and using the common notation $\alpha_s(Q)$ to denote $\bar{\alpha}_s(t)$ for $t = \ln(Q\ \ \mu)$ we have

$$\alpha_s(Q) = \frac{\alpha_s}{1 + \frac{b_0 \alpha_s \ln(Q\ \ \mu)}{2\pi}} \tag{40}$$

The solution to the RGE is easy to display in terms of the running coupling. Assuming d is the engineering dimension of F we can write $F = E^d f(E\ \ \mu\ \ g_s)$. Since f is dimensionless it can only depend on E and μ through their ratio and we have made this explicit. The solution to the RGE is

$$f(E\ \ \mu\ \ g_s) = f(1\ \ g_s(E)) \tag{41}$$

This is a remarkable result. In the case of R it means that once first order perturbation theory gives

$$R = R_0 \left(1 + \frac{1}{\pi} \alpha_s + \cdots \right) \tag{42}$$

there must be additional terms in higher order in perturbation theory which ensure that

$$R = R_0 \left(1 + \frac{1}{\pi} \alpha_s(E) + \cdots \right) \tag{43}$$

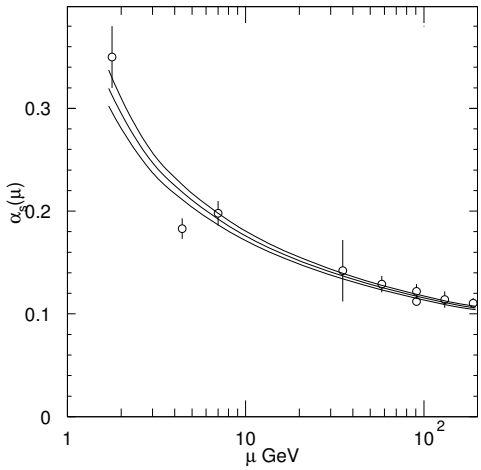

Fig. 8: Experimental confirmation of the running of the coupling constant of QCD [21]

Note that

$$\alpha_s(Q) = \frac{\alpha_s}{1 + \frac{b_0 \alpha_s \ln(Q\ \mu)}{2\pi}} = \alpha_s \sum_{n=0}^{\infty} \left(-\frac{b_0}{2\pi} \alpha_s \ln(Q\ \mu) \right)^n \tag{44}$$

So replacing $\alpha_s \to \alpha_s(E)$ introduces higher orders in α_s, leaving the first order unchanged. The higher order terms always come in the combination $\alpha_s(E) \ln(E\ \mu)$. For large E, $\alpha_s(E) \sim 1\ \ln(E\ \mu)$, so these higher order terms cannot be neglected. We have used the RGE to 're-sum the leading logs.' Had we retained one more order of α_s in our starting expression for $R = R(E\ \mu\ \alpha_s)$ and in the beta function, we would have re-summed the next-to-leading logarithms which would be suppressed relative to those retained by one power of $\alpha_s(E)$.

We see then that for any infrared safe physical process the perturbative expansion is in terms of $\alpha_s(E)$, where E is the typical energy scale of the process.[1] Note that $\alpha_s(E)$ decreases with increasing E. This property is called *asymptotic freedom*. We have already seen that the parton model description of DIS experiments indicates that strong interactions become weak if probed over short times, that is, at high energy. QCD has this necessary property built in. Experimental confirmation of this effect is now conclusive; see Fig. 8. On the other hand, as E decreases the coupling constant increases and eventually diverges at a finite value of E, called $\Lambda_{\rm QCD}$. This allows us to write

$$\alpha_s(E) = \frac{2\pi}{b_0 \ln(E\ \Lambda_{\rm QCD})} \tag{45}$$

The dimensionless coupling constant is then determined by a dimensionful number. We call this 'dimensional transmutation'. It is particularly useful to characterize the strength of the interactions by $\Lambda_{\rm QCD}$ since this quantity is renormalization group invariant.

5 Using QCD: some proton–proton scattering examples

The parton model and QCD can be used to predict the outcome of other processes. In particular we will consider here pp or $p\bar{p}$ scattering. We will gain more experience with the use of the parton model, and we will test our understanding of elementary QCD processes, like quark–gluon and gluon–gluon scattering.

[1] Things get more complicated if there are several disparate but large energy scales in the problem. The technique of effective field theories can be used to sum the different leading logs in that case. Detailed discussion is beyond the scope of these lectures.

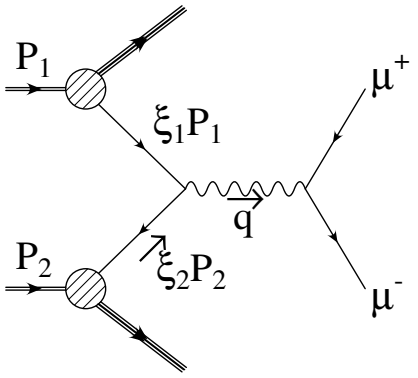

Fig. 9: Parton model picture for the Drell–Yan process. Protons with momenta P_1 and P_2 have partons with collinear momenta $\xi_1 P_1$ and $\xi_2 P_2$ which annihilate into a $\mu^+\mu^-$ pair.

Not every pp collision can be studied perturbatively. In fact, most pp collisions are soft: they produce a multitude of hadrons largely in the same direction as the original protons. These presumably arise from the exchange of a low energy gluon even if the centre of mass energy can be large. The time scale characteristic of this soft gluon exchange is not different from the typical hadronic time scale m_p^{-1}. But if we limit our attention to processes in which the particles scatter into a very large angle so that multiple products carry a large component of momentum transverse to the collision axis, $p_\perp$, then the parton–parton collision is much faster and we expect perturbative QCD to be applicable in describing the partonic process. So, if Y stands for a final state with large $p_\perp$ and X is the rest of the inclusive hadronic final state, we write

$$\sigma(p(P_1)p(P_2) \to Y + X) = \int d\xi_1 \int d\xi_2 \sum_{i\,j} f_i(\xi_1) f_j(\xi_2) \hat{\sigma}(q_i(\xi_1 P_1) q_j(\xi_2 P_2) \to Y) \tag{46}$$

We have simply used the parton model twice, once for each incident proton. To make this expression useful we need to relate the collinear momentum fractions ξ_i to observable kinematic variables and we must compute the short-distance cross-section for parton–parton scattering.

5.1 Drell–Yan

We begin with the simplest case: Drell–Yan. Here the outgoing particles with large $p_\perp$ are leptons; see Fig. 9:

$$\sigma(p(P_1)p(P_2) \to \mu^+\mu^- + X) = \int d\xi_1 \int d\xi_2 \sum_{i\,j} f_i(\xi_1) \bar{f}_i(\xi_2) \hat{\sigma}(q_i(\xi_1 P_1) \bar{q}_i(\xi_2 P_2) \to \mu^+\mu^-) \tag{47}$$

The parton cross-section is easy to compute. It is similar to the well known result for $e^+e^- \to \mu^+\mu^-$ but with the QCD novelty that one has to average over initial colours, $3 \times (1\ 3)^2$, giving

$$\hat{\sigma}(q_i(p_1)\bar{q}_i(p_2) \to \ell^+\ell^-) = \frac{4\pi\alpha^2 e_i^2}{9\hat{s}} \tag{48}$$

Sorting out the kinematics requires a little work. Experimentally only the $\mu^+\mu^-$ momenta are measured. We need to relate these to the parton fractions ξ_i. In the centre-of-mass frame,

$$\text{CM:} \qquad P_1 = E(1\ 0\ 0\ 1) \qquad P_2 = E(1\ 0\ 0\ -1) \qquad s = 4E^2 \tag{49}$$

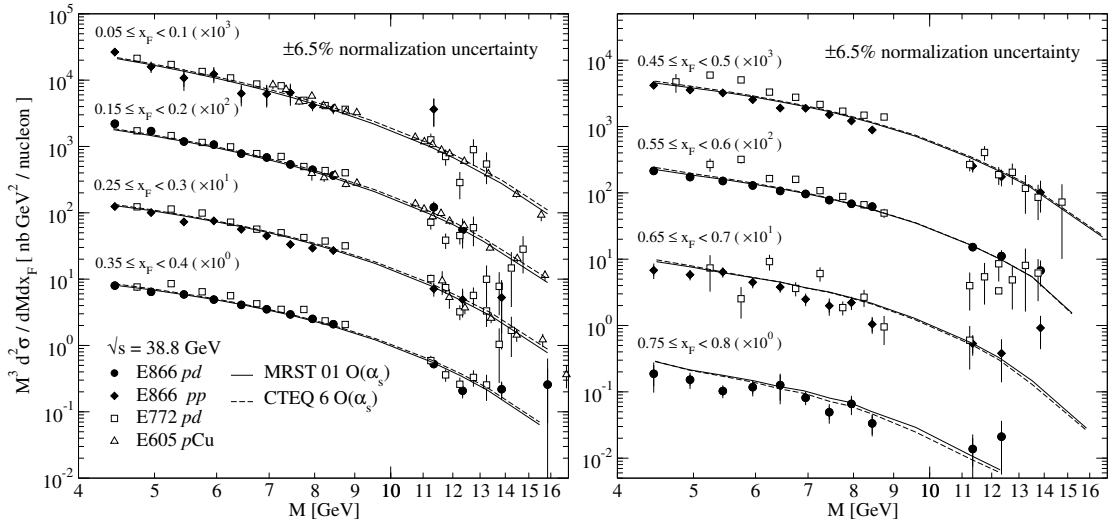

Fig. 10: Drell–Yan cross-section from the E866/NuSea collaboration and predictions from the parton model using CTEQ and MRST densities [22]. The data from the E772 and E605 displays only statistical error bars. For details on the systematic errors for E866 see Ref. [22].

The off-shell photon momentum is determined from the final state, so it is known. But it can also be expressed in terms of unknowns:

$$q = \xi_1 P_1 + \xi_2 P_2 = E(\xi_1 + \xi_2 \;\; 0 \;\; 0 \;\; \xi_1 - \xi_2) \qquad \hat{s} = q^2 = \xi_1 \xi_2 s \tag{50}$$

Since q is known, the two components q^0 and q^3 determine the fractions ξ_1 and ξ_2. The equations are customarily solved in terms of the rapidity, y, defined by

$$q^0 = \sqrt{q^2}\cosh y \qquad q^3 = \sqrt{q^2}\sinh y \tag{51}$$

Rapidity is additive under boosts in the direction of the pp axis, and therefore rapidity distributions are invariant. Solving the two simultaneous equations,

$$\xi_1 = \sqrt{\frac{q^2}{s}} e^{y} \qquad \xi_2 = \sqrt{\frac{q^2}{s}} e^{-y} \tag{52}$$

We can now write the differential cross-section in terms of the variables q^2 and y. We need the Jacobian J in $d\xi_1 d\xi_2 = J dq^2 dy$. With $J = \partial(\xi_1 \;\; \xi_2) \;\; \partial(q^2 \;\; y) = \xi_1 \xi_2 \;\; q^2$ we have, putting it all together,

$$\frac{d\sigma}{dq^2 dy}\sigma(p(P_1)p(P_2) \to \ell^+\ell^- + X) = \sum_i \xi_1 f_i(\xi_1)\xi_2 f_{\bar{i}}(\xi_2) \; \frac{4\pi\alpha^2 e_i^2}{9q^4} \tag{53}$$

Note that the cross-section depends on the quark densities but not on the gluon densities.

Results from the E866/NuSea collaboration are shown in Fig. 10. They are expressed in terms of the two variables $M \equiv \sqrt{q^2}$ and $x_F \equiv \xi_1 - \xi_2 = q^3 \;\; E = 2p_\parallel \;\; \sqrt{s}$:

$$M^3 \frac{d\sigma}{dM dx_F} = \sum_i \xi_1 f_i(\xi_1)\xi_2 f_{\bar{i}}(\xi_2) \; \frac{8\pi\alpha^2 q_i^2}{9(\xi_1 + \xi_2)} \tag{54}$$

5.2 Dijets

We can apply the same techniques to the problem of jet pair production in pp or $p\bar{p}$ scattering. Here, however, the parton porcesses $1+2 \to 3+4$ involve both quarks and gluons in the initial and final states and are mediated by QCD interactions. The final-state quark (or gluon), being coloured, is not directly observed. Instead it 'fragments' into colourless hadrons. These hadrons are mostly collinear with the fragmenting quark: they form a 'jet'. When the quark energy is degraded by multiple fragmentations, soft interactions between the two jets can neutralize the remaining colour. We need not worry about this fragmentation and colour neutralization processes if our observables are inclusive enough. We will not discuss how to define jets quantitatively in an infrared safe manner, but will assume such definition is used in convolution with our cross-section. It must be clear that, in any case, we require that the jets have large transverse momentum. We should also point out that it is extremely difficult to determine whether a jet originates from a quark or gluon, or from which particular quark flavour. It therefore makes sense to add over all possibilities in defining the dijet cross-section.

Let us begin our discussion by studying the kinematics of the parton $1 + 2 \to 3 + 4$ process. In the pp centre-of-mass frame, the incident partons have

$$p_1 = \xi_1 E(1\ 0\ 0\ 1) \qquad p_2 = \xi_2 E(1\ 0\ 0\ -1) \tag{55}$$

Characterize the momenta of outgoing partons by their rapidities and transverse momentum:

$$p_i = (p_\perp \cosh y_i\ \ \pm\vec{p}_\perp\ \ p_\perp \sinh y_i) \quad i = 3\ 4 \tag{56}$$

Again conservation of momentum gives two equations which are readily solved:

$$\xi_1 = \frac{p_\perp}{\sqrt{s}}(e^{y_3} + e^{y_4}) \qquad \xi_2 = \frac{p_\perp}{\sqrt{s}}(e^{-y_3} + e^{-y_4}) \tag{57}$$

Mandelstam variables can be computed in terms of these, e.g., $\hat{t} = -2p_1 \cdot p_3 = -2p_\perp^2 \cosh(\Delta y)e^{-\Delta y}$, where $\Delta y \equiv y_3 - y_4$. Then, retaining the angular distribution of the outgoing partons, we have

$$\frac{d\sigma}{d\hat{t}}(pp \to 3 + 4 + X) = (d\xi_1 f_1(\xi_1))(d\xi_2 f_2(\xi_2))\frac{d\hat{\sigma}}{d\hat{t}}(1 + 2 \to 3 + 4) \tag{58}$$

Changing variables to the observables (computing the Jacobian $\dfrac{\partial(x_1\ x_2\ \hat{t})}{\partial(y_3\ y_4\ p_\perp)} = \dfrac{8p_\perp^3}{s}\cosh^2(\Delta y)$, the triple differential cross-section is given by

$$\frac{d^3\sigma}{dy_3 dy_4 dp_\perp^2}(pp \to 3 + 4 + X) = x_1 f_1(x_1) x_2 f_2(x_2)\frac{d\hat{\sigma}}{d\hat{t}}(1 + 2 \to 3 + 4) \tag{59}$$

Tree-level Feynman diagrams for the elementary processes needed for the computation of the dijet cross-section are shown in Fig. 11. We will not display the computations of these cross-sections, but point out some novelties that arise in QCD (i.e., which are absent in the corresponding QED calculation).

Only diagram (a) contributes to the process $ud \to ud$. It has a factor of $T^a_{ij}T^a_{lm}$ for the vertices, where $i\ \ l$ are the initial-state colours and $j\ \ m$ the final-state colours. When we average the modulus of the amplitude $|\mathcal{M}|^2$ over initial colours and sum over final colours we encounter

$$\left(\frac{1}{3}\right)^2 \sum_{i\ j}\sum_{lm} T^a_{ij}T^a_{lm}(T^b_{ij}T^b_{lm})^* = \frac{1}{9}\mathrm{Tr}(T^aT^b)\mathrm{Tr}(T^aT^b) = \frac{1}{9}\left(\frac{1}{2}\right)^2 \delta^{ab}\delta^{ab} = \frac{2}{9} \tag{60}$$

The cross-section is just like in $e\mu \to e\mu$ but replacing $\alpha \to \alpha_s$ and including a factor of $2\ \ 9$. The $u\bar{u} \to d\bar{d}$ annihilation cross-section in diagram (c) is obtained from this by crossing, $\hat{t} \leftrightarrow \hat{s}$, in the amplitude.

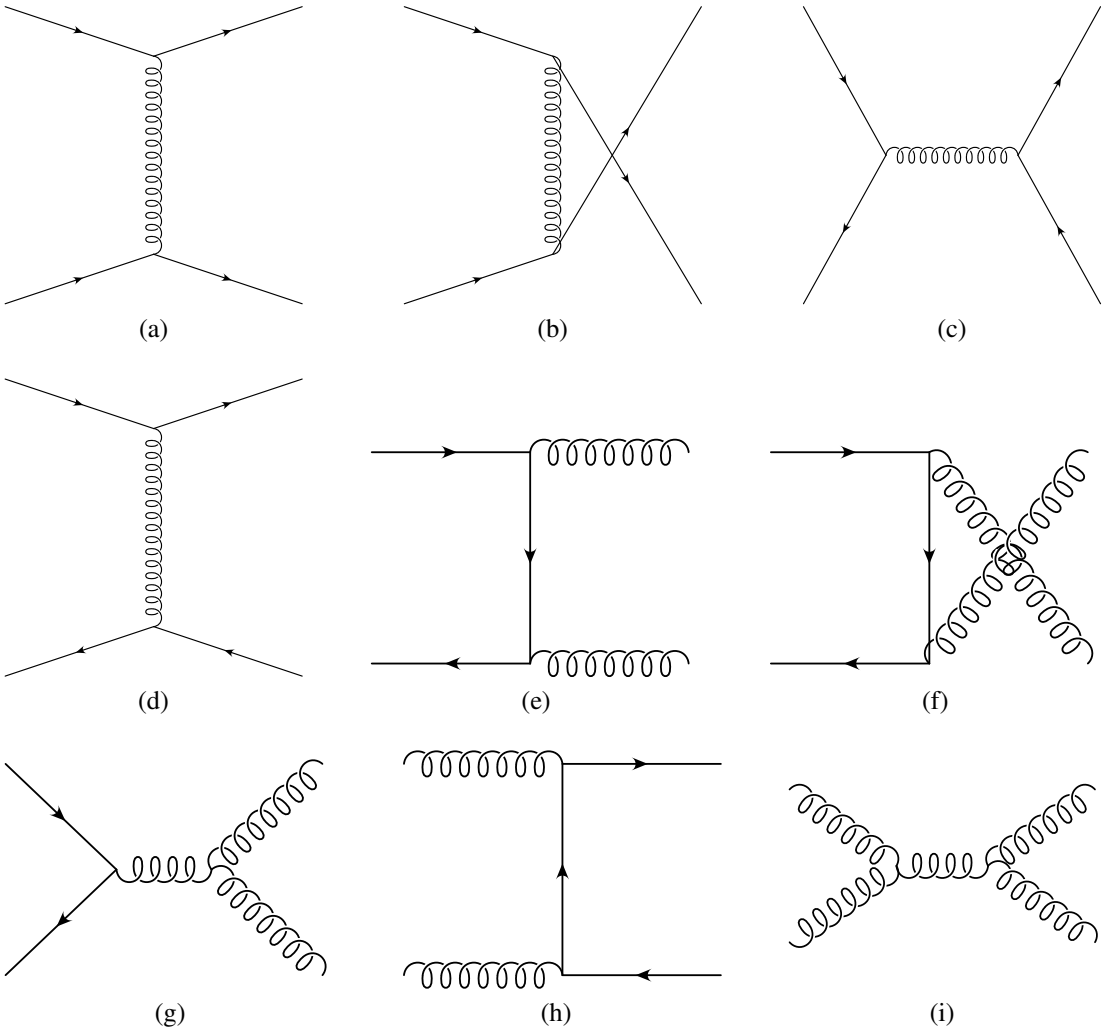

Fig. 11: Tree-level Feynman diagrams for the elementary processes needed for the computation of the dijet cross-section: (a) $qq \to qq$ t-channel, (b) $qq \to qq$ u-channel, (c) $q\bar{q} \to q\bar{q}$ s-channel, (d) $q\bar{q} \to q\bar{q}$ t-channel, (e) $q\bar{q} \to gg$ t-channel, (f) $q\bar{q} \to gg$ u-channel, (g) $q\bar{q} \to gg$ s-channel, (h) $gg \to q\bar{q}$ t-channel (u-channel not shown), and (i) $gg \to gg$ (point interaction from four-gluon vertex not shown).

The process $u\bar{u} \to u\bar{u}$ has in addition to diagram (c) also diagram (d). The square of diagram (d) is just as that of (a). There is an additional interference term. It involves the product

$$T^a_{ij} T^b_{jm} T^a_{ml} T^b_{li} = \text{Tr}\,(T^a T^b T^a T^b) = -\frac{2}{3} \tag{61}$$

and one obtains

$$\frac{d\sigma}{d\hat{t}}(u\bar{u} \to u\bar{u}) = \frac{4\pi\alpha_s^2}{9\hat{s}^2}\left[\frac{\hat{s}^2+\hat{u}^2}{\hat{t}^2} + \frac{\hat{t}^2+\hat{u}^2}{\hat{s}^2} - \frac{2}{3}\frac{\hat{u}^2}{\hat{s}\hat{t}}\right] \tag{62}$$

Here the first and second terms are from the square of diagrams (a)=(d) and (c), respectively, and the last is from interference. The computation of $uu \to uu$, from diagrams (a) and (b), is obtained from this by crossing, $u \leftrightarrow s$.

The amplitudes for $uu \to gg$ are shown in diagrams (e), (f), and (g). The first two are similar to the QED process $ee \to \gamma\gamma$, but the last one includes the three-gluon coupling characteristic of Yang–Mills

theory. The QED-like diagrams have $T^a_{ij}T^b_{jk}$ averaged (summed) over initial (final) colours:

$$\left(\frac{1}{3}\right)^2 (T^aT^b)_{ik}(T^aT^b)^*_{ik} = \frac{1}{9}\text{Tr}(T^aT^bT^bT^a) = \frac{1}{9}\left(\frac{4}{3}\right)^2 \text{Tr}(1) = \frac{16}{27} \tag{63}$$

Diagram (g) has a colour factor $T^c_{ij}f^{abc}$. Squaring and averaging (summing) over initial (final) colours:

$$\left(\frac{1}{3}\right)^2 \sum_{ijab} T^c_{ij}f^{abc}(T^d_{ij}f^{abd})^* = \frac{1}{9}\text{Tr}(T^cT^d)f^{abc}f^{abd} = \frac{1}{9}\left(\frac{1}{2}\delta^{cd}\right)(3\delta^{cd}) = \frac{1}{9}\frac{1}{2}3\cdot 8 = \frac{4}{3} \tag{64}$$

Altogether one obtains

$$\frac{d\hat{\sigma}}{d\hat{t}}(u\bar{u}\to gg) = \frac{32\pi\alpha_s^2}{27\hat{s}^2}\left[\frac{\hat{u}}{\hat{t}} + \frac{\hat{t}}{\hat{u}} - \frac{9}{4}\left(\frac{\hat{t}^2+\hat{u}^2}{\hat{s}^2}\right)\right] \tag{65}$$

The inverse process $gg \to uu$ proceeds through the same diagrams but read from right to left (for example, diagram (h) is (e) read backwards). The only difference in the cross-section is that the average over initial colour is now $(1\ \ 8)^2$, so there is a correction factor of $(3\ \ 8)^2$. The related processes $ug \to ug$ and $\bar{u}g \to \bar{u}g$ are obtained from this by crossing, $\hat{s} \leftrightarrow \hat{t}$, and an overall colour correction factor $(3\ \ 8)$.

Finally, for $gg \to gg$ there are gluon mediated processes in all three channels [the s-channel exchange is shown in diagram (i)] and a local four-gluon interaction. The laborious but straightforward calculation gives

$$\frac{d\hat{\sigma}}{d\hat{t}}(gg\to gg) = \frac{9\pi\alpha_s^2}{2\hat{s}^2}\left[3 - -\frac{\hat{u}\hat{t}}{\hat{s}^2} - \frac{\hat{s}\hat{t}}{\hat{u}^2} - \frac{\hat{s}\hat{u}}{\hat{t}^2}\right] \tag{66}$$

The result of this calculation can be compared with experiment. Figure 12 show the PDG compilation of experimental results and next-to-leading-order (NLO) theoretical curves for comparison, using CTEQ parton density functions. The normalization is somewhat uncertain. (Recall that the argument E in $\alpha_s(E)$ is not precisely fixed: the next-to-NLO calculation is required for this.) Yet we see impressive agreement with experiment: the shape is tracked over seven orders of magnitude in cross-section.

6 Scaling violations

We now turn our attention to corrections to the leading order results obtained above for DIS. While the discussion applies similarly to our other examples (Drell–Yan, dijets), we use DIS as the means to introduce and discuss the subject. While computing NLO corrections will increase the accuracy of the theoretical predictions, the motivation for discussing this here is the introduction of new effects (violations to Bjorken scaling) and new ideas (factorization, evolution equations, etc.).

Before launching into the details of the discussion, let us get a qualitative idea of what parton evolution is and how it is related to Bjorken scaling. Consider the DIS diagram in Fig. 13. A gluon has been radiated from the collinear quark before its collision with the off-shell photon. If the gluon is nearly collinear with the proton the process will simply degrade the collinear momentum fraction of the quark, from x to y in the diagram, and will add a gluon component to the proton. Near collinear emissions introduce logarithmic divergences, $\sim dp_\perp\ \ p_\perp$. So if we restrict $p_\perp < Q$, the quark density function will be modified by a Q-dependent term, $f(x) \to f(x\ \ Q) = f(x) + \alpha_s \ln(Q\ \ \mu)\,\widetilde{P}(x)$, where μ is an infrared cut-off and $\widetilde{P}(x)$ is related to the probability of emitting the gluon off a quark with momentum fraction x. As we increase the energy of our collisions, we can raise the limit Q: the cross-section will depend on Q through the parton density functions and Bjorken scaling will be slighly violated by logarithmic Q-dependence.

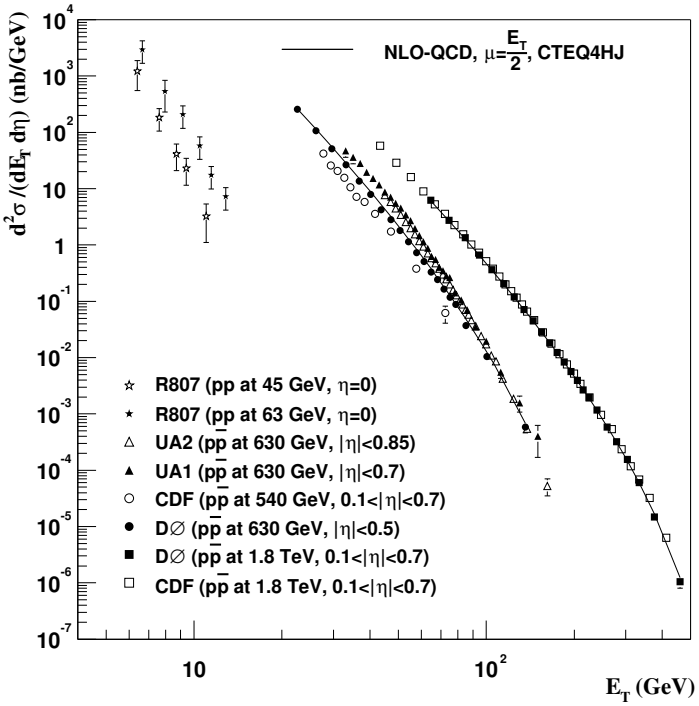

Fig. 12: Experimental results for the dijet cross-section in $p\bar{p}$ collisions and comparison with theory [21]. Comparison between different experimental results is not straightforward since different jet reconstruction algorithms were used. Theory results are NLO-QCD with CTEQ4HJ pdfs using $\mu = E_T/2$.

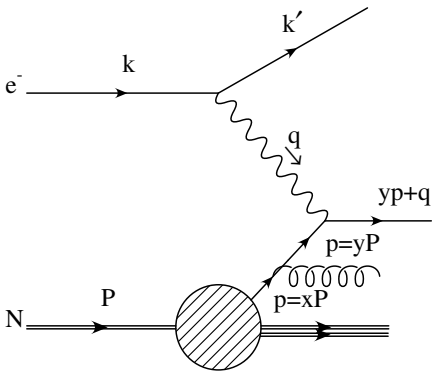

Fig. 13: Gluon radiation from struck parton in deep inelastic scattering

6.1 Factorization

In order to understand better and compute the effects of collinear emission of partons in DIS, and to generalize to the case of multiple emissions, it is useful to understand the concept of factorization. We will discuss it in the context of QED, where the computations are simpler but the conceptual issues are substantially the same. Moreover, the QED case is interesting in its own right. For example, multiple photon emission is used to measure $e\bar{e} \to Z \to \nu\bar{\nu}$. So we consider Figs. 1 and 13 but with the incoming nucleon replaced by an electron, and quarks and gluons replaced by electrons and photons. The second figure has three additional elements: an electron propagator and vertex, an emitted photon particle and the

Fig. 14: Subdiagrams in $ee \to eX$ scattering that are compared in establishing factorization

associated phase space integral. As we will see, factorization is the statement that these three elements come in as an overall factor.

To be more precise (but not very), consider the subdiagrams of Figs. 1 and 13 shown in Fig. 14. The statement of factorization is that the leading divergence at small $p_\perp$, the transverse momentum of the emitted photon, of the square of the amplitude, summed over final-state polarizations, is the product of the square of the amplitude with no photon emission and a computable factor:

$$\sum_{\text{pols}} |\mathcal{M}_1|^2 = \frac{e^2}{p_\perp^2} \widetilde{P}(z) |\mathcal{M}_0|^2 \tag{67}$$

where $\widetilde{P}(z)$ is a function of the collinear momentum fraction z only. The phase space integral for the emitted photon then gives

$$\sigma(\ell e \to \ell(e\gamma)) = \int_0^1 dz \int \frac{dp_\perp^2}{p_\perp^2} \frac{\alpha}{2\pi} \widetilde{P}(z) \sigma(\ell e \to \ell e) \tag{68}$$

Notice the similarity with the parton model. In fact, following the parton model we write

$$\sigma(\ell(k) e(p) \to \ell X) = \int_0^1 dz f_e(z) \sigma(\ell(k) e(zp) \to \ell e) \tag{69}$$

where $f_e(z)dz$ is the probability of finding an electron with longitudinal momentum fraction between z and $z + dz$ when probing an electron. It follows that

$$f_e^{(1)}(x) = \frac{\alpha}{2\pi} \ln \frac{s}{m^2} \widetilde{P}(x) \tag{70}$$

We have included a superscript to indicate this is the result of the emission of one photon, and we have performed the integral over $p_\perp$, which is logarithmic and cut-off in the infrared by the small but non-vanishing electron mass and in the ultraviolet by the largest available momentum which we simply estimate as s.

This first approximation to the electron density is wrong on several counts. First, in the limit $\alpha \to 0$ the electron density should be concentrated at $z = 1$ and be associated with no photon emission, $f^{(0)}(x) = \delta(1 - x)$. Second, the probability should be normalized, $\int dx f_e(x) = 1$, but clearly neither $f^{(1)}(x)$ nor $f^{(0)}(x) + f^{(1)}(x)$ are. As we will see, the third problem is that $\widetilde{P}(x)$ diverges as $x \to 1$. All three problems are corrected by replacing the $\widetilde{P}(x)$ by a distribution with vanishing integral, $\widetilde{P}(x) \to P(x)$, and

$$f_e(x) = \delta(1 - x) + \frac{\alpha}{2\pi} \ln \frac{s}{m^2} P(x) \tag{71}$$

The difference between $\widetilde{P}(x)$ and $P(x)$ is concentrated at $z = 1$ and can be understood as arising from another contribution of order α that we have neglected, namely the one-loop radiative correction to the γ^* vertex. As mentioned earlier, the vertex correction is not infrared safe by itself, but the sum with photon bremsstrahlung is. So the singularity at $z = 1$ in $\widetilde{P}(x)$ is associated with this infrared singularity, and is cancelled by the divergent vertex correction (which, of course, is concentrated at $z = 1$).

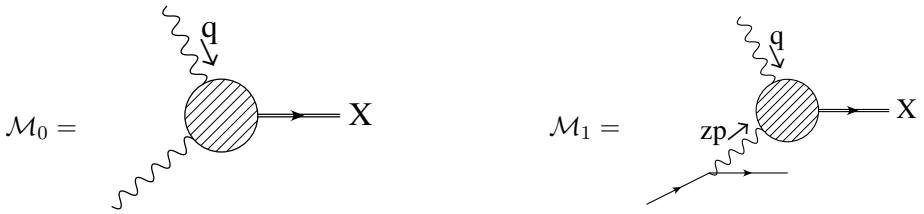

Fig. 15: Factorization and the photon content of the electron

Similarly one may consider the photon density in the electron, $f_\gamma(x)$. To this end consider the amplitudes in Fig. 15. Factorization states that the leading term at small $p_\perp$ of the final-state electron is

$$\sum_{\text{spins}} |\mathcal{M}_1|^2 = \frac{e^2}{p_\perp^2} P'(z) |\mathcal{M}_0|^2 \tag{72}$$

for some function $P'(z)$. By an argument like the one above, it follows that

$$f_\gamma(x) = \frac{\alpha}{2\pi} \ln \frac{s}{m^2}\, P'(x) \tag{73}$$

One can similarly consider photon and positron density functions. And, if the log is large as will be the case in QCD, one may wonder about resumming leading logs in these expressions. We will come back to these issues when we consider density evolution equations. For now let us see how factorization works in detail and compute the functions $P(z)$ and $P'(z)$.

To this end we will calculate (compare with the second diagram in Fig. 14)

$$\sum_{\text{spins}} \left| \quad + \quad \right|^2 \tag{74}$$

and show that in collinear limit it is proportional to

$$\sum_{\text{spins}} \left| \quad \right|^2 = e^2 \sum_{s\ s'} \bar{u}(p')\gamma^\mu u(p) \left[\bar{u}(p')\gamma^\nu u(p)\right]^* = e^2 \text{Tr}\, \left(p'\gamma^\mu p \gamma^\nu\right) \tag{75}$$

with p replaced by $p - k$. In these diagrams the off-shell photon couples to the μ component of the current and carries momentum q. We have summed over initial electron spin also. This is unnecesary but makes the computation simpler. Alternatively one can introduce a helicity projection operator and then sum over the spin without loss of generality.

For the computation we need the following kinematics. The massless electron and emitted photon momenta are

$$p^\mu = (p\ \ 0\ \ 0\ \ p) \qquad k^\mu = ((1-z)p\ \ (1-z)p\sin\theta\ \ 0\ \ (1-z)p\cos\theta) \tag{76}$$

The transverse momentum is then $k_\perp = (1-z)p\sin\theta$, which for small θ gives $\theta = k_\perp\ \ (1-z)p$. Then, the virtual electron momentum is, in the first photon emission amplitude (u-channel),

$$(p-k)^\mu = (zp\ \ -k_\perp\ \ 0\ \ zp + \frac{k_\perp^2}{2(1-z)p}) \quad \text{with virtuality} \quad \hat{u} = (p-k)^2 = -2p\cdot k = \frac{k_\perp^2}{(1-z)} \tag{77}$$

while in the second (s-channel) the virtuality $\hat{s} = (p+q)^2 = q^2 + 2q\cdot p$ is large. A divergence as $p_\perp^2 \to 0$ arises from vanishing propagator denominators, so only the u-channel graph diverges. For the square of the sum of amplitudes, divergences appear in the square of the u-channel graph and in the interference term.

The u-channel amplitude has a diverging denominator $1\ (2p\cdot k)^2$. The numerator has

$$\sum_{s\ s'\ \epsilon} \left|\bar{u}(p')\gamma^\mu(p-k)\epsilon^* u(p)\right|^2 = \sum_\epsilon \text{Tr}\left(p'\gamma^\mu(p-k)\epsilon^* p\epsilon(p-k)\gamma^\nu\right) = 2\text{Tr}\left(p'\gamma^\mu(p-k)p(p-k)\gamma^\nu\right) \tag{78}$$

In the last step we made the replacement $\sum_\epsilon \epsilon_\alpha\epsilon^*_\beta \to -g_{\alpha\beta}$, which is allowed by current conservation. Now we use the fact that $pp = 0 = kk$ and $kpk = \{k\ p\}k - pkk = 2k\cdot pk$:

$$= 2\text{Tr}\left(p'\gamma^\mu kpk\gamma^\nu\right) = 2(2k\cdot p)\text{Tr}\left(p'\gamma^\mu k\gamma^\nu\right) = 2(1-z)(2k\cdot p)\text{Tr}\left(p'\gamma^\mu p\gamma^\nu\right) \tag{79}$$

In the step before last we obtained a factor of $2p\cdot k$, which softens the divergence as $k_\perp^2 \to 0$. For that reason we neglect $k_\perp$ in the remaining factor, which allows us to write $k \approx (1-z)p$ in the last step. Note that the remaining trace is precisely the amplitude of the process with no photon emission (times $2p\cdot k$).

The interference calculation is similar, but since there is only one diverging power of $1\ 2p\cdot k$ from the start we can replace k by $(1-z)p$ in the numerator. So we have

$$\begin{aligned}\sum_{s\ s'\ \epsilon} \bar{u}(p')\gamma^\mu(p-k)\epsilon^* u(p)\left[\bar{u}(p')\epsilon^*(p'+k)\gamma^\nu u(p)\right]^* &= 2\text{Tr}\left(p'\gamma^\mu(p-k)(p'+k)\gamma^\nu p\right)\\ &= 2z\text{Tr}\left(p'\gamma^\mu pp'\gamma^\nu p\right)\end{aligned} \tag{80}$$

and it is easy to show that the last trace is $\text{Tr}\left(p'\gamma^\mu pp'\gamma^\nu p\right) = -2p\cdot p'\text{Tr}\left(p'\gamma^\mu p\gamma^\nu\right)$.

Combining results from the u-channel and the interference terms we obtain

$$\sum|\mathcal{M}_1|^2 = -\frac{2e^2}{2k\cdot p}\left(\frac{1+z^2}{1-z}\right)\text{Tr}\left(p'\gamma^\mu p\gamma^\nu\right) = \frac{2e^2}{k_\perp^2}\left(\frac{1+z^2}{z}\right)\text{Tr}\left(p'\gamma^\mu(p-k)\gamma^\nu\right) \tag{81}$$

The trace factor is the same as in Eq. (75), which shows factorization. To complete the calculation of the cross-section we integrate over phase space. But the phase space for everything but the collinear photon is already included in the lower order cross- section. So we integrate over the photon phase space only. The integration over the direction in the transverse plane is trivial. Recalling that $k^3 \approx (1-z)p$,

$$\int\frac{d^3k}{(2\pi)^3 2k^0} = \int\frac{\pi dk_\perp^2\, pdz}{(2\pi)^3 2(1-z)p} \tag{82}$$

So integrating our factorization relation over phase space $d\Phi(X)$ of the final state plus the photons, we have

$$\int d\Phi(X+\gamma)\sum|\mathcal{M}_1|^2 = \int\frac{dk_\perp^2}{k_\perp^2}dz\frac{\alpha}{2\pi}\left(\frac{1+z^2}{1-z}\right)\frac{1}{z}\int d\Phi(X)\sum|\mathcal{M}_0|^2 \tag{83}$$

Finally the cross-section requires factors of the flux of speed of light particles and of the inverse of the energies of the incident particles. These are common except for the energy of the electron, which is p on the left-hand side and zp on the right-hand side. The explicit factor of $1\ z$ accounts for this difference, and we finally arrive at Eq. (68) with the explicit result,

$$\widetilde{P}(z) = \left(\frac{1+z^2}{1-z}\right) \tag{84}$$

One can perform an analogous computation for a collinear electron emitted from an electron, and a photon that goes on to a hard collision. It can be shown, however, that $P'(z) = \widetilde{P}(1-z)$:

$$P'(z) = \widetilde{P}(1-z) = \left(\frac{1+(1-z)^2}{z}\right) \tag{85}$$

The electron and photon density functions of the electron are then

$$\begin{aligned} f_e(x) &= \delta(1-x) + \frac{\alpha}{2\pi}\ln\frac{s}{m^2}\left(\frac{1+x^2}{(1-x)_+} + \frac{3}{2}\delta(1-x)\right) \\ f_\gamma(x) &= \frac{\alpha}{2\pi}\ln\frac{s}{m^2}\left(\frac{1+(1-x)^2}{x}\right) \end{aligned} \tag{86}$$

We have performed the integral over transverse momentum, cut-off at small $k_\perp$ by the electron mass and at large $k_\perp$ by some typical large scale in the problem $\sqrt{s}$ that dictates the maximum of $k_\perp$. Also, we have included in the large bracket a term concentrated at $x = 1$, $C\delta(1-x)$, with coefficient $C = 3\ \ 2$. This is determined by regulating the divergence at $x = 1$. Replace the factor $1\ \ (1-x)$ by a 'plus'-distribution, $1\ \ (1-x)_+$ defined by

$$\int_0^1 dx\,\frac{f(x)}{(1-x)_+} = \int_0^1 dx\,\frac{f(x)-f(1)}{(1-x)} \tag{87}$$

Applying this to f_e we have

$$\int_0^1 dx\,\frac{1+x^2}{(1-x)_+} = \int_0^1 dx\,\frac{x^2-1}{(1-x)} = -\frac{3}{2} \tag{88}$$

In order for f_e to remain normalized we must choose $C = 3\ \ 2$.

6.2 Evolution

Factorization is the basis for re-summing the leading logs in DIS. We have isolated the large log arising from the singularities in the emission of a collinear parton, and expressed the result in terms of the lowest order process. The idea in performing the re-summation is to repeat the procedure with additional collinear partons. Since factorization holds, when we add over all collinear emissions we will obtain the product of the lowest order term and a factor which is the sum of increasing powers of $\alpha\ln(s\ \ m^2)$.

To see how this works, consider the two collinear photon emission diagram in Fig. 16. The two electron propagators have denominators $-2p\cdot k_2 \sim k_{2\perp}^2$ and $-2p\cdot(k_1+k_2) \sim k_{1\perp}^2 + k_{2\perp}^2$. These will give rise to a product of two logs if in the second we can neglect $k_{2\perp}^2$ relative to $k_{1\perp}^2$. For that region of phase space the transverse momentum integrals will give

$$\left(\frac{\alpha}{2\pi}\right)^2 \int_{m^2}^{s} \frac{dk_{1\perp}^2}{k_{1\perp}^2} \int_{m^2}^{k_{1\perp}^2} \frac{dk_{2\perp}^2}{k_{2\perp}^2} \tag{89}$$

$$= \frac{1}{2}\left(\frac{\alpha}{2\pi}\right)^2 \ln^2\frac{s}{m^2} \tag{90}$$

Similarly, with n emissions, the region of transverse momentum integration $k_{1\perp}^2 \gg k_{2\perp}^2 \gg \cdots \gg k_{n\perp}^2$, where k_1 is closest to the hard scattering and k_n is farthest from it gives $1\ \ n!(\alpha\ln(s\ \ m^2)^n$.

The computation along these lines becomes difficult once we attempt to include mixed processes with collinear emission of both photons and electrons. There is a simpler way to proceed by setting up an equation whose solution is the sum. To this effect we think of the collinear emissions as a continuous evolution process, as a function of the transverse momentum of the electron constituent. Replace the density function $f(x)$ by $f(x\ \ Q)$, the probability of finding a parton in the electron with longitudinal

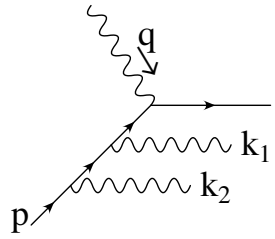

Fig. 16: Two collinear photons emitted from the parton before the hard scattering. This diagram gives a second order contribution $\sim (\alpha \ln(s/m^2))^2$.

momentum fraction x and transverse momentum up to Q, $k_\perp \leq Q$. By 'finding' here we mean that when we probe the electron the hard scattering will occur with the parton with those characteristics, because of mutiple collinear radiation.

We then ask, how does $f(x\ Q)$ change as we increase Q to $Q + \Delta Q$? An electron in $f_e(x\ Q)$ may radiate a photon with $Q < k_\perp < Q + \Delta Q$. This will contribute to $f_\gamma(x\ Q + \Delta Q)$. Recall that the differential probability for an electron to turn into a photon (radiating a collinear electron) is

$$\frac{\alpha}{2\pi}\frac{dk_\perp^2}{k_\perp^2}P'(z) \tag{91}$$

So the probability $f_\gamma(x\ Q + \Delta Q)dx$ to find a photon in the electron with transverse momentum up to $Q + \Delta Q$ is the sum of the probability $f_\gamma(x\ Q)dx$ of finding it with transverse momentum up to Q and the probability that a photon with transverse momentum between Q and $Q + \Delta Q$ is emitted from an electron. If this electron has momentum fraction y and the photon has a fraction z of this, then

$$f_\gamma(x\ Q + \Delta Q)dx = f_\gamma(x\ Q)dx + \left[\frac{\alpha}{2\pi}\frac{\Delta Q^2}{Q^2}P'(z)dz\right] f_e(y\ Q)dy \tag{92}$$

Note that the photon momentum fraction must be x, so $zy = x$, or $y = x\ z$ and $dy = dx\ z$. Integrating over all z such that $y \leq 1$, we have, finally,

$$\frac{d}{d\ln Q}f_\gamma(x\ Q) = \int_x^1 \frac{dz}{z}\frac{\alpha}{\pi}P'(z)f_e(\frac{x}{z}\ Q) \tag{93}$$

This is the first of the evolution equations.

One can similarly find an equation for $f_e(x\ Q)$. However, one must consider the possibility of starting from a photon [from $f_\gamma(x\ Q)$] and radiating an electron or a positron. Factorization works just as before, and the splitting probability can be determined straightforwardly. We leave this as an exercise for the reader.

The complete set of evolution equations is named after Gribov and Lipatov, who first derived them. Writing $P_{xy}(z)$ [sometimes also written $P_{x\to y}(z)$] for the probability that parton y splits off parton x with longitudinal momentum fraction z, we have the Gribov–Lipatov equations:

$$\begin{aligned}
Q\frac{d}{dQ}f_e(x\ Q) &= \frac{\alpha}{\pi}\int_x^1 \frac{dz}{z}\left(P_{ee}(z)f_e(\frac{x}{z}\ Q) + P_{e\gamma}(z)f_\gamma(\frac{x}{z}\ Q)\right)\\
Q\frac{d}{dQ}f_{\bar{e}}(x\ Q) &= \frac{\alpha}{\pi}\int_x^1 \frac{dz}{z}\left(P_{ee}(z)f_{\bar{e}}(\frac{x}{z}\ Q) + P_{e\gamma}(z)f_\gamma(\frac{x}{z}\ Q)\right)\\
Q\frac{d}{dQ}f_\gamma(x\ Q) &= \frac{\alpha}{\pi}\int_x^1 \frac{dz}{z}\left(P_{ee}(z)[f_e(\frac{x}{z}\ Q) + f_{\bar{e}}(\frac{x}{z}\ Q)] + P_{\gamma\gamma}(z)f_\gamma(\frac{x}{z}\ Q)\right)
\end{aligned} \tag{94}$$

We have included a density function for the positron, $f_{\bar{e}}(x)$, since the photon can split into either an electron or a positron when a collinear positron or electron is radiated. By charge conjugation invariance the splitting functions for the positron are equal to those of the electron. The splitting functions are

$$\begin{aligned} P_{ee}(z) &= \frac{1+z^2}{(1-z)_+} + \frac{3}{2}\delta(1-z) \\ P_{\gamma e}(z) &= \frac{1+(1-z)^2}{z} \\ P_{e\gamma}(z) &= z^2 + (1-z)^2 \\ P_{\gamma\gamma}(z) &= -\frac{2}{3}\delta(1-z) \end{aligned} \tag{95}$$

The splitting function for a photon into a photon is trivial since the photon is not charged (it does not interact with itself). The delta function contribution arises from inisisting that f_γ be properly normalized.

To find the density functions of partons in the electron we need to solve the Gribov–Lipatov equations with the following initial conditions at $Q = m$:

$$f_e(x\ Q) = \delta(1-x) \qquad f_\gamma(x\ Q) = 0 \qquad f_{\bar{e}}(x\ Q) = 0 \tag{96}$$

If one is interested instead in collisions of a photon (or a positron), the corresponding density functions of partons in the photon (or positron) are obtained by solving the same equations but with initial conditions $f_\gamma(x\ m) = \delta(1-x)$, $f_e(x\ m) = 0$ and $f_{\bar{e}}(x\ m) = 0$ [or $f_{\bar{e}}(x\ m) = \delta(1-x)$, $f_e(x\ m) = 0$ and $f_\gamma(x\ m) = 0$].

6.3 GLAP evolution equations

We can now return to the question of re-summation of leading logs in QCD. We can repeat the same arguments and calculations as in QED, with some modifications. First, we cannot trust the calculation of $f(x\ Q)$ at low Q. But for large Q, we can trust our calculation of the change in $f(x\ Q)$ from Q to $Q + \Delta Q$. Therefore we may trust evolution equations, but we will have to resort to experiment to determine the initial conditions.

There are obvious changes in the calculation that arise from colour factors. More interesting is a novel contribution arising from the fact that gluons can interact with themselves. Therefore one can split a gluon into gluons, $g \to gg$, giving rise to a non-trivial contribution to the splitting function P_{gg}.

The full set of Gribov–Lipatov–Altarelli–Parisi (GLAP) evolution equations is [24–26]

$$\begin{aligned} Q\frac{d}{dQ}f_i(x\ Q) &= \frac{\alpha_s(Q)}{\pi}\int_x^1 \frac{dz}{z}\left(P_{qq}(z)f_i(\frac{x}{z}\ Q) + P_{qg}(z)f_g(\frac{x}{z}\ Q)\right) \\ Q\frac{d}{dQ}f_{\bar{i}}(x\ Q) &= \frac{\alpha_s(Q)}{\pi}\int_x^1 \frac{dz}{z}\left(P_{qq}(z)f_{\bar{i}}(\frac{x}{z}\ Q) + P_{qg}(z)f_g(\frac{x}{z}\ Q)\right) \\ Q\frac{d}{dQ}f_g(x\ Q) &= \frac{\alpha_s(Q)}{\pi}\int_x^1 \frac{dz}{z}\left(P_{gq}(z)\sum_i[f_i(\frac{x}{z}\ Q) + f_{\bar{i}}(\frac{x}{z}\ Q)] + P_{gg}(z)f_g(\frac{x}{z}\ Q)\right) \end{aligned} \tag{97}$$

where the sum in the last line is over quark flavours, $i = u\ d\ s$ and we have guessed that the appropriate scale for α_s is of order Q.

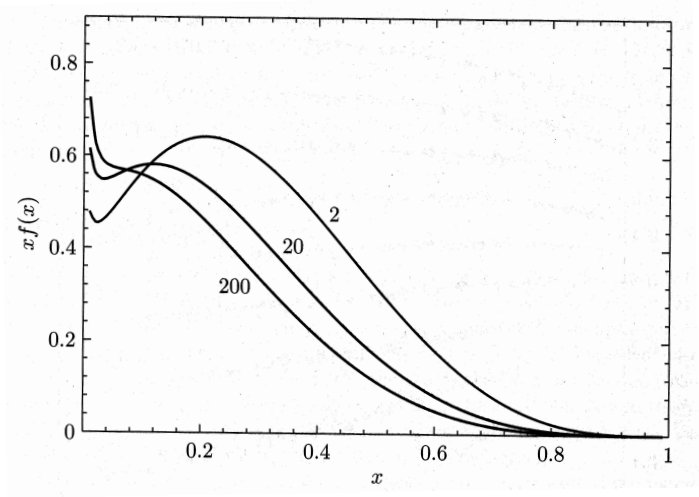

Fig. 17: GLAP evolution of a u-quark CTEQ density in the proton from the starting point at $Q = 2$ GeV to $Q = 20$ GeV and $Q = 200$ GeV. Taken from the text by Peskin and Schroeder [15].

The splitting functions in QCD include the appropriate colour factors and the interesting process of a gluon splitting into gluons:

$$\begin{aligned} P_{qq}(z) &= \frac{4}{3}\left[\frac{1+z^2}{(1-z)_+} + \frac{3}{2}\delta(1-z)\right] \\ P_{gq}(z) &= \frac{4}{3}\left[\frac{1+(1-z)^2}{z}\right] \\ P_{qg}(z) &= \frac{1}{2}\left[z^2+(1-z)^2\right] \\ P_{gg}(z) &= 6\left[\frac{1-z}{z} + \frac{z}{(1-z)_+} + z(1-z) + \left(\frac{11}{12} - \frac{n_f}{18}\right)\delta(1-z)\right] \end{aligned} \tag{98}$$

In practice the GLAP equations are solved numerically, starting from a complete set of evolution equations obtained at some low Q (but large enough that perturbative evolution is valid) from fitting to experiment. We expect that as Q increases there will be more splitting and the functions will populate the lower x region. This is illustrated in Fig. 17, taken from the text by Peskin and Schroeder [15], showing the evolution of a u-quark CTEQ density in the proton from the starting point at $Q = 2$ GeV to $Q = 20$ GeV and $Q = 200$ GeV.

An important, built-in feature of the evolution equations is that they preserve the sum rules for the density functions. Indeed, it is easy to check that

$$Q\frac{d}{dQ}\int_0^1 dx\,[f_i(x\ Q) - f_{\bar{i}}(x\ Q)] = 0 \tag{99}$$

and

$$Q\frac{d}{dQ}\int_0^1 dx\,x[\sum_i (f_i(x\ Q) + f_{\bar{i}}(x\ Q)) + f_g(x\ Q)] = 0 \tag{100}$$

and therefore that if the initial conditions satisfy the flavour and momentum sum rules, then so do the density functions at any Q.

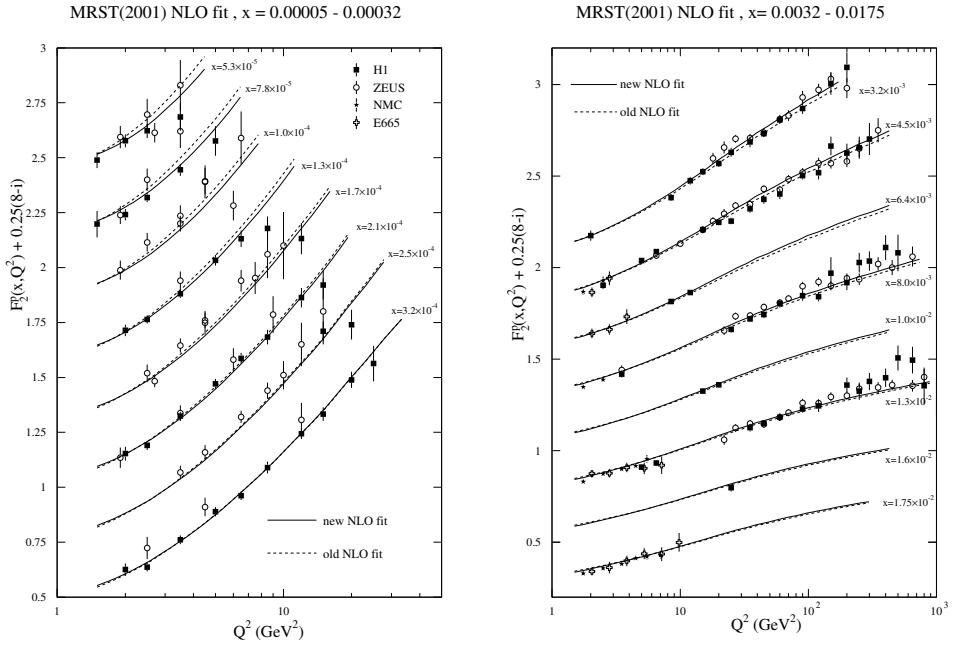

Fig. 18: DIS results of four experiments compared with the NLO fit of the MRST2001 parton densities [23]. Plotted is $F_2(x,Q^2) = \sum_i q_i^2\, x f_i(x,Q^2)$ as a function of Q^2 for different bins in x. The x bins are displaced vertically by 0.25 for display purposes. The dashed line displays the MRST99 parton densities fit.

We have managed to re-sum the leading logs that arise in the process of collinear emission associated with a hard scattering. The parton model is essentially still valid, with the caveat that the parton densities have Q dependence that can be calculated through solution of the GLAP equations. Bjorken scaling is therefore not exact, but is only violated by a mild logarithmic dependence. If Q varies over many decades this effect should be substantial. This is seen in DIS experiments at very high energy. For example, Fig. 18 compares the results of four experiments with the NLO fit of the MRST parton densities. This is displayed as a function of Q^2 for each bin in x. It is seen that the Q^2 evolution is more rapid the smaller the value of momentum fraction x, which is expected since the small x bins are being populated as one evolves in Q.

Acknowledgements

I would like to thank the conference organizers, and in particular the School Directors, Egil Lillestøl and Alberto Sanchez-Hernandez, for the opportunity to participate in this wonderful school. It comes as no surprise that a school run by a Mexican and a Swiss was both picturesque and run like clockwork. The surprise was that Alberto carried the big stick while Egil played the piano. Thanks also to the support staff. And many thanks to the discussion session leaders, Alejandro Ayala, Helio Nogima, Diego Harari and Marta Losada, who helped the students keep up with the vigorous pace of the lectures. This work was supported in part by the U.S. Dept. of Energy, under grant DOE-FG03-97ER40546.

References

[1] A. H. Mueller, *Perturbative Quantum Chromodynamics* (World Scientific, Singapore, 1989).

[2] M. K. Gaillard and B. W. Lee, Phys. Rev. Lett. **33** (1974) 108.

[3] F. J. Gilman and M. B. Wise, Phys. Rev. D **20** (1979) 2392.

[4] N. Isgur and M. B. Wise, Adv. Ser. Direct. High Energy Phys. **10** (1992) 549.

[5] B. Grinstein, Ann. Rev. Nucl. Part. Sci. **42** (1992) 101.

[6] G. T. Bodwin, E. Braaten and G. P. Lepage, 'Rigorous QCD predictions for decays of p wave quarkonia', arXiv:hep-ph/9211253.

[7] C. W. Bauer, S. Fleming and M. E. Luke, Phys. Rev. D **63** (2001) 014006 [arXiv:hep-ph/0005275].

[8] Y. L. Dokshitzer, arXiv:hep-ph/0306287, CERN report cernrep/2002-002.

[9] V. Braun, *Prepared for European School of High-Energy Physics (ESHEP 2000), Caramulo, Portugal, 20 Aug - 2 Sep 2000*, CERN report cernrep/2001-003.

[10] W. J. Stirling, CERN-OPEN-2000-296 *7th European School of High-Energy Physics, Casta-Papiernicka, Slovak Republic, 22 Aug - 4 Sep 1999*.

[11] M. L. Mangano, *Prepared for 1998 European School of High-Energy Physics, St. Andrews, Scotland, 23 Aug - 5 Sep 1998*.

[12] G. Altarelli, arXiv:hep-ph/0204179.

[13] R. K. Ellis, FERMILAB-CONF-94-410-T, *Presented at TASI '94, Boulder, Colorado, May 29 - Jun 24, 1994*.

[14] G. Sterman, ITP-SB-91-55, *Based on lectures given at the Theoretical Advanced Study Institute in Elementary Particle Physics, Boulder, Colorado, Jun 2-28, 1991*.

[15] M. E. Peskin and D. V. Schroeder, *An Introduction To Quantum Field Theory* (Addison-Wesley, Reading, Mass., 1995).

[16] F. Halzen and A. D. Martin, *Quarks And Leptons: An Introductory Course In Modern Particle Physics* (Wiley, New York, 1984).

[17] S. Pokorski, *Gauge Field Theories*, Cambridge Monographs On Mathematical Physics (CUP, Cambridge, 1987).

[18] R. P. Feynman, Phys. Rev. Lett. **23** (1969) 1415.

[19] J. D. Bjorken and E. A. Paschos, Phys. Rev. **185** (1969) 1975.

[20] H. L. Lai *et al.*, Phys. Rev. D **51** (1995) 4763 [arXiv:hep-ph/9410404].

[21] K. Hagiwara *et al.* [Particle Data Group Collaboration], Phys. Rev. D **66** (2002) 010001.

[22] J. C. Webb *et al.* [NuSea Collaboration], arXiv:hep-ex/0302019.

[23] A. D. Martin, R. G. Roberts, W. J. Stirling and R. S. Thorne, Eur. Phys. J. C **23** (2002) 73 [arXiv:hep-ph/0110215].

[24] V. N. Gribov and L. N. Lipatov, Yad. Fiz. **15** (1972) 781 [Sov. J. Nucl. Phys. **15** (1972) 438].

[25] Y. L. Dokshitzer, (in Russian), Sov. Phys. JETP **46** (1977) 641 [Zh. Eksp. Teor. Fiz. **73** (1977) 1216].

[26] G. Altarelli and G. Parisi, Nucl. Phys. B **126** (1977) 298.